AGU PUBLICATIONS

Global Biogeochemical Cycles

RESEARCH ARTICLE
10.1002/2015GB005327

Key Points:
- Seasonal reversal in the sign of NCP drives positive feedback on NCC in the summer and negative feedback in the winter
- Seasonal net dissolution in waters supersaturated with respect to aragonite
- Net loss of reefal substrate due to ocean acidification is already occurring

Supporting Information:
- Table S1
- Table S2
- Figure S1
- Text S1

Correspondence to:
C. Langdon,
clangdon@rsmas.miami.edu

Citation:
Muehllehner, N., C. Langdon, A. Venti, and D. Kadko (2016), Dynamics of carbonate chemistry, production, and calcification of the Florida Reef Tract (2009–2010): Evidence for seasonal dissolution, *Global Biogeochem. Cycles*, *30*, doi:10.1002/2015GB005327.

Received 7 DEC 2015
Accepted 5 APR 2016
Accepted article online 2 MAY 2016

Dynamics of carbonate chemistry, production, and calcification of the Florida Reef Tract (2009–2010): Evidence for seasonal dissolution

Nancy Muehllehner[1], Chris Langdon[1], Alyson Venti[1], and David Kadko[2]

[1]Rosenstiel School of Marine and Atmospheric Science, University of Miami, Miami, Florida, USA, [2]Applied Research Center, Applied Research Center, Florida International University, Miami, Florida, USA

Abstract Ocean acidification is projected to lower the Ω_{ar} of reefal waters by 0.3–0.4 units by the end of century, making it more difficult for calcifying organisms to secrete calcium carbonate while at the same time making the environment more favorable for abiotic and biotic dissolution of the reefal framework. There is great interest in being able to project the point in time when coral reefs will cross the tipping point between being net depositional to net erosional in terms of their carbonate budgets. Periodic in situ assessments of the balance between carbonate production and dissolution that spans seasonal time scales may prove useful in monitoring and formulating projections of the impact of ocean acidification on reefal carbonate production. This study represents the first broad-scale geochemical survey of the rates of net community production (NCP) and net community calcification (NCC) across the Florida Reef Tract (FRT). Surveys were performed at approximately quarterly intervals in 2009–2010 across seven onshore-offshore transects spanning the upper, middle, and lower Florida Keys. Averaged across the FRT, the rates of NCP and NCC were positive during the spring/summer at 62 ± 7 and 17 ± 2 mmol m^{-2} d^{-1}, respectively, and negative during the fall/winter at -33 ± 6 and -7 ± 2 mmol m^{-2} d^{-1}. The most significant finding of the study was that the northernmost reef is already net erosional (-1.1 ± 0.4 kg $CaCO_3$ m^{-2} yr^{-1}) and midreefs to the south were net depositional on an annual basis (0.4 ± 0.1 kg $CaCO_3$ m^{-2} yr^{-1}) but erosional during the fall and winter. Only the two southernmost reefs were net depositional year-round. These results indicate that parts of the FRT have already crossed the tipping point for carbonate production and other parts are getting close.

1. Introduction

Predicting the future of carbonate reefal building is of growing importance as ocean acidification threatens the coral reefal habitat. The rapid rise in atmospheric carbon dioxide drives greater CO_2 absorption by the oceans, changing its carbonate chemistry within the surface layers [*Sabine et al.*, 2004]. While the majority of lab studies find that a decrease in aragonite saturation state (Ω_{ar}) causes a reduction in rates of skeletal formation [*Chan and Connolly*, 2013], it is not easy to translate these results into predictions for net calcification at the community scale. The reason is that net community calcification represents a complex balance between producers and destroyers of calcium carbonate with many players operating at different trophic levels, functioning in different physical, chemical, and biological settings.

Predictions of when reefs will switch from net calcification to net dissolution span the near future such as when pCO_2 reaches 500–560 ppm at midcentury[*Hoegh-Guldberg et al.*, 2007; *Silverman et al.*, 2009; *Yates and Halley*, 2006] to the end of the century [*Andersson et al.*, 2007; *Shaw et al.*, 2012]. However, these predictions seldom incorporate the feedback effects of reefal community metabolism on the carbonate chemistry of the overlying water. The processes of photosynthesis, respiration, calcification, and dissolution on the reefal impact the carbonate chemistry of reefal waters by altering the amount of dissolved organic carbon (DIC) and total alkalinity (TA). As coastal coral reefs alter the carbonate chemistry of incoming oceanic water it can influence the Ω_{ar} value and potentially alter the time frame for when a reefal may experience net dissolution [*Shaw et al.*, 2012]. However, community metabolism (i.e., photosynthesis/respiration and calcification/dissolution) affects the flux of carbon in coastal waters differently depending on the reefal system [*Kleypas et al.*, 2011]. For example, models of varying benthic community composition show that photosynthesis on the reefs of Moorea can result in increased downstream Ω_{ar} [*Kleypas et al.*, 2011]. Alternatively, models of reefal flat systems in Australia

find that large tidal cycles, high rates of photosynthesis/respiration, and predicted increases in the seawater Revelle factor can create large swings in pCO_2, resulting in reefs that will experience intermittent Ω_{ar} under saturation sooner than expected [*Shaw et al.*, 2013]. Unfortunately, limited field data on the feedback between carbonate chemistry and benthic metabolism currently limit our ability to predict how these factors interact and thus how reefal dissolution rates in different reefal systems may shift in the future [*Silverman et al.*, 2007b; *Bates et al.*, 2010; *Shamberger et al.*, 2011; *Silverman et al.*, 2012]. Overall, the range of predictions for net reefal dissolution reflects the challenges inherent in understanding the relationships between benthic metabolism, calcification, and the changing carbonate chemistry of our oceans. Tying the nature of Ω_{ar} oscillations to net community calcification is an imperative to predicting reefal growth and identifying threshold Ω_{ar} for net calcification on different reefs as ocean acidification continues [*Atkinson and Cuet*, 2008].

The seasonally reoccurring reefal dissolution observed in this study is unprecedented, with prior reports of dissolution both rare, and occurring almost exclusively for short periods of time at night [e.g., *Barnes and Devereux*, 1984; *Yates and Halley*, 2003; *Silverman et al.*, 2007a, 2007b; *Shamberger et al.*, 2011]. In general, net dissolution on reefs is expected when ocean acidification results in undersaturated water. However, despite surface water column Ω_{ar} of 2.49 to 3.53, low-saturation state in pore waters does affect reefal structures, as is suspected to be the case the in the poorly cemented reefal framework in the eastern Pacific [*Manzello et al.*, 2008]. For instance pore water within the reefal substrate can rapidly become undersaturated due to the carbon dioxide produced by microbial remineralization of organic material [*Andersson and Gledhill*, 2012; *Walter and Burton*, 1990; *Burdige et al.*, 2010]. This process can also be enhanced by increased oxygen supply from sea grass rhizomes [*Burdige and Zimmerman*, 2002; *Burdige et al.*, 2010]. While minor dissolution is generally considered to be naturally occurring in shallow reefal waters [*Yates and Halley*, 2006], the tipping point at which net community calcification ceases will vary substantially across reefal environments [*Andersson and Gledhill*, 2012], due to highly variable factors such as organic matter content, mineral composition, grain size, sediment permeability, and porosity [*Burdige and Zimmerman*, 2002].

Regional assessments of community calcification that are both spatially and temporally robust are vital to create regional Ω_{ar} thresholds for net reefal calcification in an acidifying ocean [*Andersson and Gledhill*, 2012]. While there is a wealth of field data on reefal calcification in different regions, the spatial scale is often on the order of meters to a few kilometers or the time scale is on the order of hours to days without consideration of seasonal variability [*Bates et al.*, 2010]. In addition, the inherent physical and biological differences between reefal systems will result in different reefs displaying very different susceptibilities to net reefal dissolution under similar Ω_{ar} conditions [*Andersson and Gledhill*, 2012]. Aragonite saturation state and net community calcification typically correlate well within a reefal system, but the slope of the relationship and thus the tipping point to net dissolution for different reefal systems range from Ω_{ar} of 1 to 4.5 [*Shamberger et al.*, 2011]. Current modeling efforts are not sufficiently constrained to take the widely varying factors influencing net dissolution rates into account and thus are unable to accurately ascribe risk in varying systems. By expanding our regional field data to encompass different reefal systems and their seasonal oscillations in calcification/production, we can increase our predictive power and better identify regional thresholds for reefal growth as ocean acidification intensifies.

This study uses changes in carbonate chemistry combined with reefal water residence times calculated from radiochemical tracer measurements (Be-7 and Th-234) to provide temporally integrated rates of net community metabolism. By surveying across 200 km of the Florida Reef Tract, we assess how the biological processes of production/respiration and calcification/dissolution alter the carbonate chemistry of reefal waters both spatially and temporally across the Florida Reef Tract. We present evidence from a 2 year time period on this subtropical coral reef that net dissolution is already occurring regularly on a seasonal basis, suggesting that the system may be operating very close to its carbonate balance (tipping point). The data presented here substantiate the idea that accurately predicting the effects of ocean acidification requires (1) an understanding of regional carbonate dynamics and (2) an understanding of the biological and physical processes that can drive carbonate chemistry changes in these systems.

2. Methods

2.1. Site Description

This study was conducted from May of 2009 to December of 2010 along ~200 km of the Florida Reef Tract (FRT) from north of Biscayne National Park to the Looe Key National Marine Sanctuary (Figure 1). This reefal

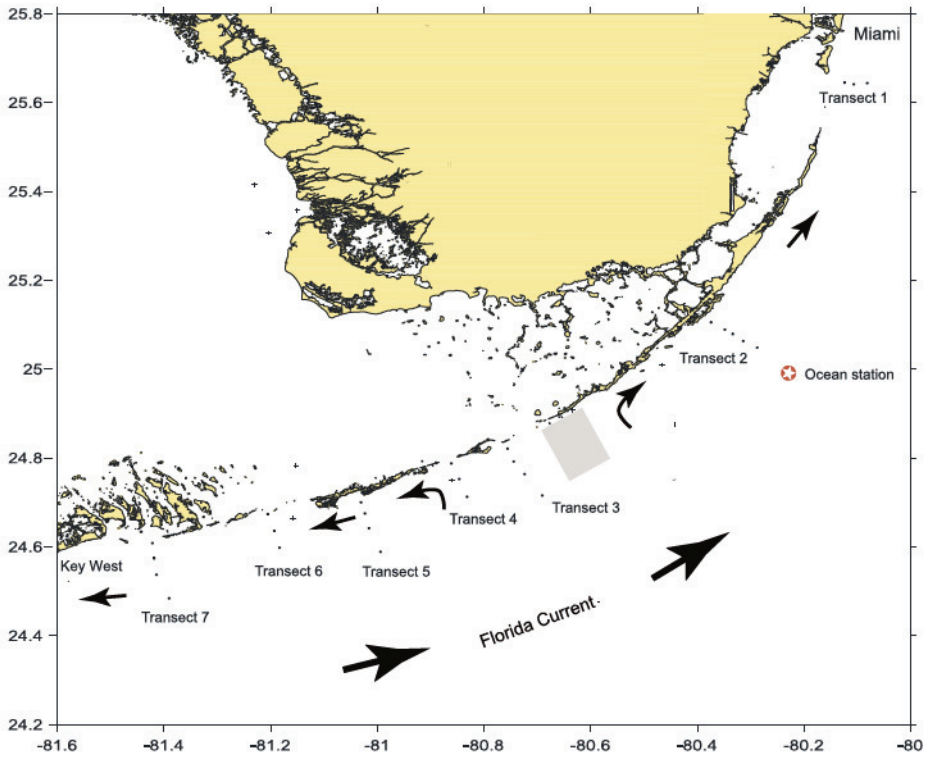

Figure 1. Map of the study area showing the locations of the stations making up the seven transects. The location where the samples for the ocean end-member were collected is shown by the starred symbol. The arrows indicate the direction and relative rates of long-term water flow [*Lee et al.*, 2002]. The gray box represents the approximate footprint (9 km × 10 km) of the alkalinity anomaly-residence time method employed in this study.

system supports a productive community with extensive sea grass beds and patch reefs lying adjacent to the string of keys facing the Atlantic Ocean. The inshore region (<2 km from shore) consists of bands of sea grass habitat interrupted by channels. The midshelf region (2–6 km offshore) includes patch reefs, sea grass beds, and hard bottom [*Burman et al.*, 2012]. The outer edge of the shelf (~8 km offshore) is defined by the reefal crest, sitting at a depth range of 2 to 20 m. Waters moving onto the FRT originate from the northward flowing Florida Current [*Lee and Williams*, 1999]. Circulation on the shelf on a subtidal time scale can be separated into subregions [*Lee et al.*, 2002]. In the lower Florida Keys, where the coastline is directed east-west, the alignment with the prevailing winds results in a mean westward coastal countercurrent, with an onshore component in the upper layer and offshore in the lower layer. The upper Florida Keys, oriented in a more north-south direction, are characterized by onshore winds that result in weak northward flow. The middle Florida Keys, where the curvature of the coastline is greatest, is a transitional region in terms of wind and Florida Current forcing. The physical processes described above result in the creation of a counterclockwise recirculation system or gyre over much of the lower and middle Florida Keys with mean flows in the 2–10 cm s^{-1} range [*Lee and Williams*, 1999]. Wind-driven Ekman transport forces onshore flow at the surface and offshore at the bottom across much of the FRT, creating a recirculation system along the cross-shelf axis. The result is a physical circulation system that is conducive to the retention of larvae and relatively long water residence time. Wind-driven offshore Ekman transport at the surface and onshore transport at the bottom (i.e., classic coastal upwelling) is rare along the southern half of the east Florida coast [*Taylor and Stewart*, 1959]. Based on tide gauge records in Miami and Key West one instance of upwelling at the Miami station and three instances at the Key West station were reported over a 13 year period. Breaking internal tides can drive high-frequency upslope flows of cooler, saltier water from below the thermocline seaward of the reef up onto the reefal platform on the time scale of 1–20 min [*Leichter et al.*, 2003]. This process is thought to be a source of nutrients to the reef and could cause short-term perturbations in the TA and DIC water properties. However, a careful examination of temperature records from National Data Buoy Center and National Oceanographic Data Center thermographs deployed at reefal floor depths at sites in the upper, middle, and lower Florida Keys

(Fowey Rocks, Molasses Reef, and Sand Key) revealed no evidence of high-frequency temperature variability events during any of the cruises making up this study.

Recent mapping surveys show sea grass beds cover up to 55% of the 3141 km^2 Florida Key area [*Lidz et al.*, 2007] with macroalgae covering up to 56% of some northern reefal areas in summer months [*Lirman and Biber*, 2000]. Calcifying organisms in the community include crustose coralline algae, calcifying macroalgae, foraminifera, and corals [*Burman et al.*, 2012; *Koch et al.*, 2012]. Areal coverage of reefal building corals in patch reefs, inshore, and offshore reefs (excluding hard bottom areas) is estimated at 2% to 7% [*Soto et al.*, 2011].

2.2. Sampling and Chemical Analysis

Seven cruises were conducted on the R/V *F.G. Walton Smith* at roughly 90 day intervals (09 April, 09 August, 09 October, 09 December, 10 May, 10 October, and 10 December). Water samples were collected along seven transects comprised of three to five stations, with the innermost station being 1–3 km offshore and the outermost station at 4.8–10.3 km offshore (Figure 1). Discrete water samples were collected from ~3 m depth from either the ship's flow through system or a conductivity-temperature-depth rosette deployed from the R/V *F. G. Walton Smith* oceanographic vessel. For our net community calcification (NCC) and net community production (NCP) calculations we assumed that a single measurement of TA and DIC taken at middepth was representative of the entire water column, i.e., that the water column was well mixed. This assumption was checked periodically by collecting samples at the top and bottom of the water column. Occasionally, differences of ±10 μmol/kg were observed but the average difference was ±1.8 μmol/kg or on the same order as the precision of our measurements. Measuring TA and DIC at multiple depths at each of the 200 stations occupied on this project would have been prohibitively time-consuming to collect and analyze.

Samples were placed in 250 mL bottles filled to rim and poisoned with 100 μL mercuric chloride to halt biological perturbation. TA was determined in triplicate (30–40 mL per analysis) by potentiometric titration with HCl using an automated open-cell Gran titration [*Dickson et al.*, 2007]; precision was 0.17% or ±2–3 μmol kg^{-1}. DIC samples from 2009 were analyzed by coulometry [*Dickson et al.*, 2007, SOP6] coupled to a single-operator multiparameter metabolic analyzer (SOMMA). DIC samples collected in 2010 were analyzed using an Apollo SciTech DIC analyzer (AS-C3, Apollotech, USA). Precision of the SOMMA-coulometer system was 0.2%, while the Apollo SciTech averaged a precision of ~0.5%. Accuracy of TA and DIC was checked against certified seawater reference material [*Dickson et al.*, 2003]. Determination of pCO_2, pH_T, and aragonite saturation state (Ω_{arag}) were calculated as a function of the measured temperature, salinity, TA, and DIC using the program CO2SYS [*Lewis and Wallace*, 1998]; dissociation constants for carbonic acid were determined by *Mehrbach et al.* [1973] as refit by *Dickson and Millero* [1987], and the dissociation constant for boric acid was determined by *Dickson* [1990]. Salinity and temperature was obtained from a Sea-Bird thermosalinograph connected to the ship's uncontaminated seawater line. In addition, an underway pCO_2 analyzer system was present on the Walton Smith during three cruises through NOAA's Vessels of Opportunity Program. Analyses of Be-7 and Th-234 were performed using the methods given in *Venti et al.* [2012] and briefly described in the supporting information section.

All TA and DIC values were normalized to a common salinity of 35 by multiplying by the factor (35/*S*), where *S* was the measured salinity at each station. The idea behind the normalization is to correct for small changes in TA and DIC that are due to evaporation and precipitation. No correction was made for an alternate end-member such as river or groundwater. This was based on the fact that *Cai et al.* [2010] found that the TA-salinity relationship in the Florida Straits was highly linear and had an intercept of 310 μmol kg^{-1}, indicating minimal freshwater input of TA. No study has looked at the carbonate chemistry of groundwater upwelling onto the FRT. However, the possibility that groundwater might be contributing nutrients has received considerable attention. *Reich et al.* [2002] injected dye into injection wells located on the bayside of Key Largo and observed that under certain meteorological conditions that caused sea level to be higher on the bayside, the dye would appear after approximately 16 days in wells located on the oceanside. It should be noted that the wells were located with 50–80 m of the shoreline. *Szmant and Forrester* [1996] looked at water column and sediment interstitial water nutrient concentration distribution patterns and observed that while levels were elevated immediately along the coastline, beyond 0.5 km of the shore, the concentrations were back to typical oligotrophic baseline levels. More work on the flux of groundwater onto the reefs and the carbonate chemistry of

that water needs to be done, but at the present time there is no strong evidence that it is a significant contribution to the TA and DIC budgets on the FRT.

In the following sections when we use the term spring/summer we are speaking collectively of data collected during spring and summer cruises (09 April, 09 August, and 10 May) and use fall/winter to collectively refer to data collected during the fall and winter cruises (09 October, 09 December, 10 October, and 10 December). We introduce the terms upper, middle, and lower to refer to transects of stations aggregated by location along the reefal tract from north to south (upper—transects 1 and 2, middle—transects 3–5, and lower—transects 6 and 7). We also have aggregated stations according to distance from shore. We refer to stations located between 1.1 and 3.3 km as inner and those located between 4.3 and 10.3 km as outer.

2.3. Calculating Net Production and Calcification Rates

Changes in seawater carbonate chemistry between upstream (ocean source water) and downstream (reefal water) can be used to calculate net community production (NCP) and net community calcification (NCC) rates via the alkalinity anomaly method [*Smith and Key*, 1975]. This method assumes that the precipitation of 1 mol of $CaCO_3$ reduces the DIC by 1 mol and the TA by 2 mol since each mol of Ca^{2+} taken up removes two equivalents of charge. Deviations from this simple stoichiometry can arise in certain environments if organic carbon production is coupled to significant uptake of NO_3^- (increases TA) or NH_4^+ (decreases TA) [*Brewer and Goldman*, 1976]. However, on coral reefs the concentrations of NO_3^- and NH_4^+ are typically $<0.5\ \mu mol\ kg^{-1}$ and their contributions to the measured change in TA can safely be ignored [*Kinsey*, 1978; *Smith and Atkinson*, 1983]. The change of TA in water moving over the benthos relative to the TA of the ocean source water provides a measure of net $CaCO_3$ production (i.e., calcification-dissolution). Accordingly, net community calcification, NCC (mmol $CaCO_3\ m^{-2}\ d^{-1}$), can be calculated as

$$NCC = -0.5\ h\rho\frac{\Delta n\mathrm{TA}}{\tau} \tag{1}$$

where ΔnTA is the difference in salinity-normalized total alkalinity between the reef ($n\mathrm{TA}_r$) and ocean ($n\mathrm{TA}_o$) station ($\mu mol\ kg^{-1}$), ρ is the seawater density ($kg\ m^{-3}$), h is the water depth (m), and τ is the water residence time (days).

DIC is affected by calcification, dissolution, photosynthesis, respiration, and gas exchange. Net community production, NCP (mmol $CaCO_3\ m^{-2}\ d^{-1}$), can be calculated using the changes in DIC after taking into account NCC and gas exchange:

$$NCP = -h\rho\frac{(\Delta n\mathrm{DIC} - 0.5\Delta n\mathrm{TA})}{\tau} - kS(pCO_{2w} - pCO_{2a}) \tag{2}$$

where ΔnDIC is the difference in salinity-normalized dissolved inorganic carbon between the reef ($n\mathrm{DIC}_r$) and ocean ($n\mathrm{DIC}_o$) station ($\mu mol\ kg^{-1}$). The term $kS(pCO_{2w} - pCO_{2a})$ approximates the CO_2 gas exchange flux, where k is the gas transfer velocity, S is the solubility of CO_2 calculated as a function of temperature and salinity, and $(pCO_{2w} - pCO_{2a})$ is the difference in pCO_2 (µatm) between the surface reefal water and the atmosphere. The other terms are as defined in equation (1). The wind speed parameterization of *Ho et al.* [2006] was used to calculate k. Average wind speed for the month in which each cruise occurred was obtained from the NOAA National Data Buoy Center for the closest site. Weekly average wind speed would have been preferred but was not available. Average monthly wind speeds for the seven cruises exhibited little variability ($4.1–5.3\ m\ s^{-1}$). The incorporation of air-sea gas exchange lowered the NCP rates by an average of $2.7 \pm 2.0\ mmol\ m^{-2}\ d^{-1}$ or 14%.

Samples used to establish the carbonate chemistry of the ocean end-member were collected at the ocean station (24.9950°N, 80.2317°W) located 19.1 km offshore (red symbol in Figure 1). Measured nTA averaged 2292 ± 12 (mean ± SD) $\mu mol\ kg^{-1}$. A search of the Global Ocean Data Analysis Product database found that oceanic waters in the Caribbean/West Atlantic (25.0–28.0°N, 90–79.3°W) have uniform nTA properties in the upper 200 m ($2295 \pm 6\ \mu mol\ kg^{-1}$). This means that episodic events like wind-driven upwelling, breaking internal tides, or passage of eddies are unlikely to alter the $n\mathrm{TA}_o$ of the waters flowing up onto the reefal platform, and this in turn means that calculations of calcification and dissolution based on the alkalinity anomaly method will be robust. nDIC measured at the ocean station exhibited more cruise to cruise

variability, 1945–2041 μmol kg^{-1}. *Bates et al.* [2012], based on 20 years of observations of ocean carbonate chemistry at the Bermuda Time Series station, observed a consistent seasonal swing in *n*DIC (~1937–1971 μmol kg^{-1}) between summer and winter and no significant seasonal change in *n*TA (2286 ± 12 μmol kg^{-1}). The larger-amplitude swing in *n*DIC at our ocean station may indicate that seasonality in $n\mathrm{DIC}_o$ is greater off the east coast of Florida than near Bermuda. For this study we measured $n\mathrm{DIC}_o$ during each cruise so the temporal variability in this parameter does not necessarily translate into an error in our measurements of NCP. However, this is a matter that deserves more attention when studies like this one are repeated. $n\mathrm{DIC}_o$ should be measured at multiple offshore points along the FRT and as a function of depth so it will be possible to assess the consequence of upwelling introducing water with a higher $n\mathrm{DIC}_o$ up onto the reefal platform. For now the estimates of NCP in this study should be regarded as less robust than the measurements of NCC because $n\mathrm{DIC}_o$ is more variable both in time and in depth. If upwelling due to breaking internal tides were to happen during a sampling trip it would be expected to bias NCP high during the spring/summer because it would increase the delta *n*DIC calculation, while during the fall/ winter it would bias the NCP low because it would decrease the delta *n*DIC. This should not be considered a serious limitation of this study because (1) thermograph records do not indicate the occurrence of such events during any of the sampling trips and (2) the focus of this study was on accurate measurements of the balance between calcification and dissolution.

For each calculation of NCP or NCC, the residence time of the water measured at that station was used. In cases where τ was not measured at a particular station the average τ for that transect line was used. In the case of transect line 6 (Bahia Honda) where no measurements of τ were made, rates of NCC and NCP were computed by using the average τ from lines 5 and 7. Rates of NCC and NCP were averaged by line, and then the average of each line was averaged by season to obtain the average winter and summer rates for the entire reefal tract. This was in turn averaged to obtain the annual average NCC and NCP of the entire reefal tract.

2.4. Residence Time

Residence time (τ) per station was obtained using a technique based on measurements of Be-7 and Th-234 [*Venti et al.*, 2012]. Details on the methodology of the Be-7 tracer method used for this study can be found in Table S1 in the supporting information. Residence time was calculated on 5 of the 7 cruises and a total 33 times for 15 different stations across the reefal tract during 2009 and 2010. Inshore stations were measured a total of 15 times, while offshore stations were measured a total of 14 times.

The calculation of reefal water residence times is based on the difference in Be-7 activities between oceanic and reefal waters. Be-7 is a naturally occurring, cosmogenic radionuclide with a half-life of 53.3 days that enters the ocean via precipitation followed by homogenization within the surface mixed layer [*Kadko and Olson*, 1996]. Of relevance to the present application, the open ocean inventory of Be-7 is diluted throughout the mixed layer, while the same inventory is concentrated over the much shallower reefal platform. This results in higher Be-7 activities over the reef as compared to the offshore water. The persistence of this difference in Be-7 activity between the open ocean and reefal waters can be used to estimate the residence time of water over the reef. For example, a high flushing rate, or short residence time, would tend to diminish the difference in Be-7 activity, whereas a long residence time would result in a higher difference between the ocean and the reef. *Venti et al.* [2012] compared the Be-7 method with the salinity method and showed that residence times computed by the two methods were comparable but the Be-7 method yielded a more precise estimate. The Be-7 method is appropriate for determining residence times occurring over time scales of days to weeks, thus providing a suitable tracer for estimating residence times in shallow reefal environments [*Venti et al.*, 2012].

2.5. TA-DIC Diagrams

TA-DIC diagrams have been used for many years to help visualize how coral reefs alter the carbonate chemistry of the overlying seawater [*Kawahata et al.*, 1997; *Suzuki et al.*, 2003; *Watanabe et al.*, 2006]. When the salinity normalized values of TA and DIC from water samples collected over a coral reef over some period of time are displayed on a TA-DIC diagram it is common to observe that the points fall along a line radiating to the left or right from a point that represents the mean TA and DIC properties of the ocean source water. TA-DIC diagrams can be divided into quadrants centered on the ocean point (Figure 2). Data points falling in the lower left quadrant are the result of positive rates of NCP and NCC. The closer the data points fall along a line

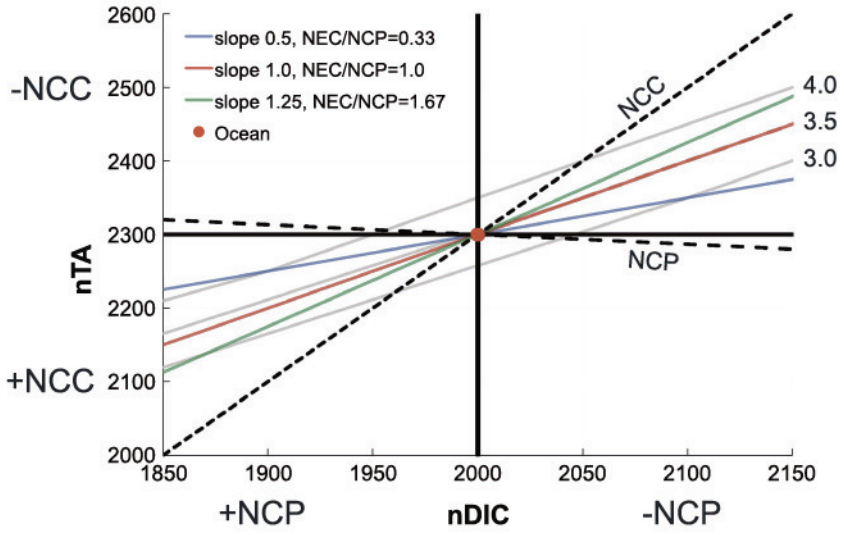

Figure 2. TA-DIC diagram showing the Ω_{ar} 3.0, 3.5, and 4.0 isolines (gray dashed lines) and metabolic process vectors (blue, red, and green lines) representing the range of slopes encountered in the present study. The red symbol represents a hypothetical ocean end-member. The heavy black horizontal and vertical lines divide the diagram into quadrants where the processes NCC and NCP are positive or negative.

with a slope of 0 the more organic carbon production dominates over inorganic carbon production (calcification). If inorganic carbon production completely dominates, then the data points will fall along a line with a slope of 2.0 because for each mole of $CaCO_3$ formed two equivalents of charge are removed for each mole of DIC in the form of CO_3^{2-}. In practice, data points from reefal studies typically fall somewhere between these two extremes. The data points on the TA-DIC diagram can be thought of as vectors that have a magnitude and a direction. These vectors can be resolved using standard rules of vector math into two component vectors (a NCC vector and a NCP vector). This is what we are doing when we say that $NCC = -0.5 \times \Delta TA$ and $NCP = -(\Delta DIC - 0.5\Delta TA)$. *Suzuki et al.* [2003] derived a very useful equation that relates the slope of the TA-DIC relationship ($\Delta TA/\Delta DIC$) to the NCC:NCP ratio:

$$\frac{NCC}{NCP} = \frac{1}{\left(\frac{2}{m} - 1\right)} \tag{3}$$

where m is the slope of the vector representing a single data point or the slope formed by an assemblage of data points (vectors). Equation (3) is undefined when $m = 2$ but is well behaved for the range of slopes typically observed in reefal studies, i.e., $m = 0.3$–1.3.

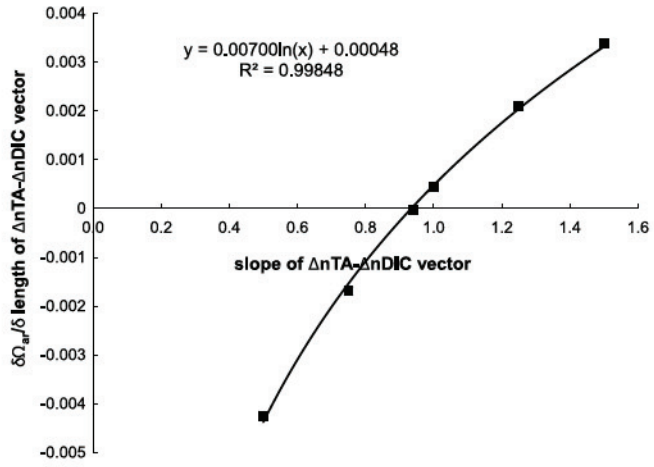

Figure 3. Curvilinear relationship between the slope of the metabolic vector and the amount that Ω_{ar} is elevated or depressed per unit metabolic vector length.

The other quadrant of interest on TA-DIC diagrams is the upper right corresponding to negative rates of NCP and NCC. In this quadrant data points represent TA and DIC values in excess of the ocean source water. If data points fall along a line with a slope near zero we know that the breakdown of organic matter (respiration) is the dominant process. If the points fall along a line with a slope of 2 we know that dissolution of carbonate is the dominant process. Equation (3) can be used to determine the NCC:NCP ratio if the slope falls somewhere between the two extremes.

Data points falling in the upper left quadrant would indicate that NCP is positive and NCC is negative. Conversely, data points in the lower right quadrant would indicate that NCP is negative and NCC is positive. Interestingly, it is uncommon to observe data points in these quadrants suggesting that these combinations of biogeochemical processes (photosynthesis and dissolution) and (respiration and calcification) may be rare on reefs.

As described in the previous paragraphs, TA-DIC diagrams can be used to draw inferences about the sign and relative balance between biogeochemical processes on a reef. If the vector is directed to the left and down, then a healthy reef with positive rates of NCC and NCP is indicated. The closer the slope of the vector is to 1 the closer the two processes are to being in balance. If the slope is less than 1, then NCP > NCC. If the slope is greater than 1, then NCP < NCC. If the vector is directed to the right and up a reef that is losing biomass (living or detrital; NCP < 0) and reefal framework (NCC < 0) is indicated. This may be natural on diel or even seasonal time scales, but it is obviously unsustainable on an annual basis or longer. Again, if the slope of the vector is less than 1, then NCP > NCC (i.e., respiration exceeds dissolution), and if the slope is greater than 1, then NCP < NCC.

There is great interest in how coral reefs are responding to changes in pH, Ω_{ar}, and pCO_2 as a result of ocean acidification. Invasion of anthropogenic CO_2 is steadily driving down the pH and Ω_{ar} of reefal waters on an annual basis. However, biogeochemical processes (i.e., photosynthesis and dissolution) on coral reefs have been shown to elevate pH and Ω_{ar} on diel and seasonal time scales to the potential advantage of the corals and the process of calcification in particular. At other times biogeochemical processes (i.e., respiration and calcification) can acidify the water and worsen chemical conditions for calcifiers. TA-DIC diagrams can be used to study these interactions if the diagrams are overlain with isolines of pH, Ω_{ar}, or pCO_2. The TA-DIC diagram in Figure 2 has been overlain with isolines for Ω_{ar}. The lines are not perfectly straight over the domain of TA and DIC encountered on reefs but are well approximated by lines with a slope of 0.94–0.95. According to equation (3) data points falling along a line with a slope of 0.94 corresponds to a NCC:NCP ratio of 0.89. This means that when the processes of photosynthesis and calcification or respiration and dissolution are nearly in balance the processes cause very little change in Ω_{ar}. The red line in Figure 2 indicates this condition. If the balance of processes is in favor organic carbon production or respiration (e.g., $m = 0.5$ and NCC:NCP = 0.33), it can be seen (blue line in Figure 2) that the vector representing this condition cuts across the isolines at an angle. Vectors directed into the lower left quadrant with a slope <0.94 elevate the Ω_{ar} of the reefal water relative to the ocean source water and vectors with a slope <0.94 directed into the upper left quadrant depress Ω_{ar} relative to the ocean. If instead the balance is in favor of inorganic carbon production or dissolution (e.g., $m = 1.25$ and NCC:NCP = 1.67), the vectors cut across the isolines in the opposite direction (green line in Figure 2). The result is that vectors directed in the lower left quadrant with a slope >0.94 depress Ω_{ar} and vectors with a slope >0.94 directed in the upper right quadrant elevate Ω_{ar} relative to the source water.

An equation that allows the calculation of the change in Ω_{ar} for any TA-DIC vector can be derived by making a graph of the computed change in Ω_{ar} for a vector of unit length as a function of the slope of that vector (Figure 3). A logarithmic function of the form $y = 0.00700 \times \ln(m) + 0.00048$ provided an excellent fit to the data over the range of slopes that are common in reefal studies ($r^2 = 0.998$). The complete expression that allows the calculation of $\Delta\Omega_{ar}$ for any TA-DIC vector is given by

$$\Delta\Omega_{ar} = (0.00700\ln(m) + 0.00048)\sqrt{\Delta n\mathrm{TA}^2 + \Delta n\mathrm{DIC}^2} \quad (4)$$

where ln(m) is the natural log of the slope of the TA-DIC vector and the radical term is the length (L) or magnitude of the metabolic vector in units of $\mu mol\,kg^{-1}$ with ΔnTA and ΔnDIC as previously defined in section 2.2. It should be noted that the magnitude of the metabolic vector is a function of the rates of NCC and NCP and the water residence time.

2.6. Statistics

Analysis of variance (ANOVA) was conducted using JMP version 11.0.0 on response variables ΔnTA, ΔnDIC, Ω_{arag}, NCC, and NCP, with season, location, and distance from shore as fixed factors. Where the ANOVAs detect significant effects, Tukey's honest significant difference (HSD) post hoc multiple mean comparison tests were performed to see where the differences lay. Correlation tests were run between nTA and nDIC,

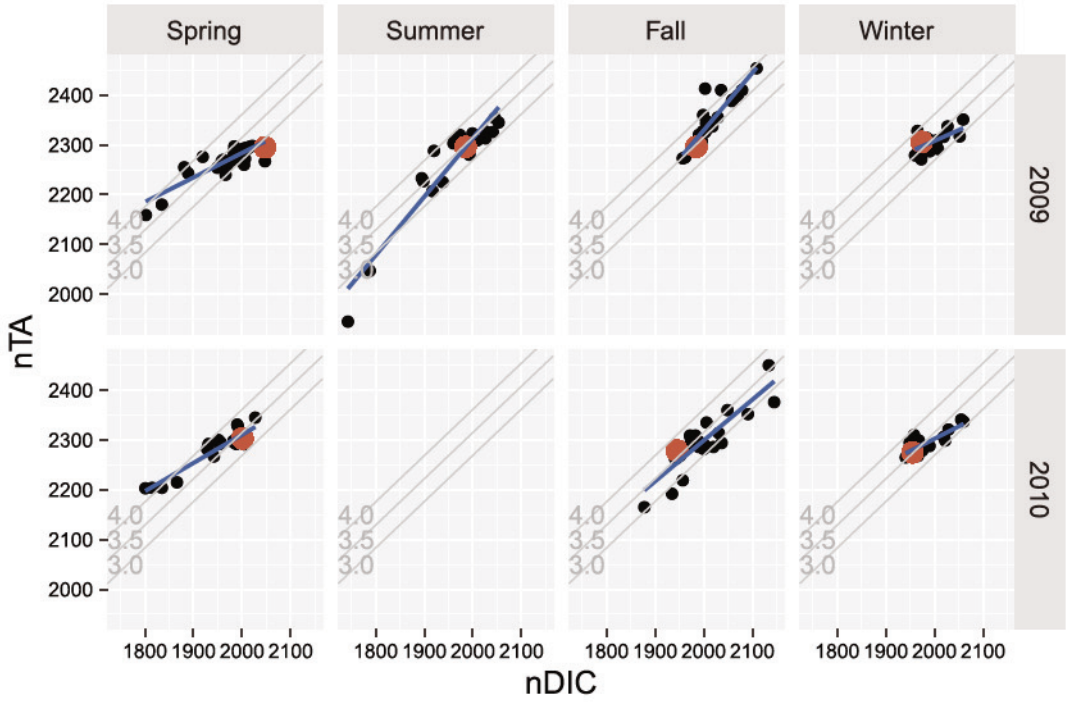

Figure 4. *n*TA-*n*DIC diagrams by season and year. The red symbol denotes the properties of the ocean end-member. The blue lines show the best fit linear regression. The gray lines show the Ωar isolines. The black arrows represent the metabolic processes indicated.

Ω_{arag} and NCC, and NCP and NCC and tested for a linear fit using the R routine lmodel2. The significance level for all tests was $\alpha = 0.05$.

3. Results

3.1. Temporal and Spatial Trends in Δ*n*TA and Δ*n*DIC

The main observables in this study were Δ*n*TA and Δ*n*DIC. These are the surplus/deficits in *n*TA and *n*DIC relative to the ocean end-member values of nTA_o and $nDIC_o$. They are of importance because they provide a temporally and spatially averaged geochemical signal of the net amount of $CaCO_3$ precipitated or dissolved and organic matter produced or metabolized on the seafloor below as described in section 2.3. Histograms of Δ*n*TA and Δ*n*DIC are shown in Figure 4. Values of Δ*n*TA ranged from $-150\ \mu mol\ kg^{-1}$ to $+100\ \mu mol\ kg^{-1}$, and values of Δ*n*DIC ranged from $-250\ \mu mol\ kg^{-1}$ to $+200\ \mu mol\ kg^{-1}$.

Before considering the Δ*n*TA or Δ*n*DIC data in detail we first examine the value at which the deltas are statistically significantly different from zero. Since the deltas are determined from the difference between reef and ocean end-member TA or DIC measurements we can use the equation for finding the standard error of the difference between two means:

$$SE_{dif} = \sqrt{\frac{SD_r^2}{n} + \frac{SD_o^2}{n}} \tag{5}$$

where *SEdif* is the standard error of the difference in Δ*n*TA or Δ*n*DIC, SD_r is the standard deviation of the reefal water TA or DIC analyses, SD_o is the standard deviation of the ocean TA or DIC analyses, and $n = 3$ since the analyses were performed in triplicate. If a typical value of 3.0 is assumed for the SD of the TA and DIC analyses (see section 2.3), then $SEdif = 2.45$ and the difference will be statistically significant if Δ*n*TA or Δ*n*DIC $> 2.132 \times 2.45 = 5.2\ \mu mol\ kg^{-1}$, where 2.132 is the critical *t* value for $df = 4$.

In Figures 5a and 5b, measurements of Δ*n*TA and Δ*n*DIC that fall in the not significant band between −5.2 and +5.2 are indicated by the black bars and those that are significantly negative are in white and those that are significantly positive in dark gray. Just 13% of the Δ*n*TA measurements and 12% of the Δ*n*DIC of the

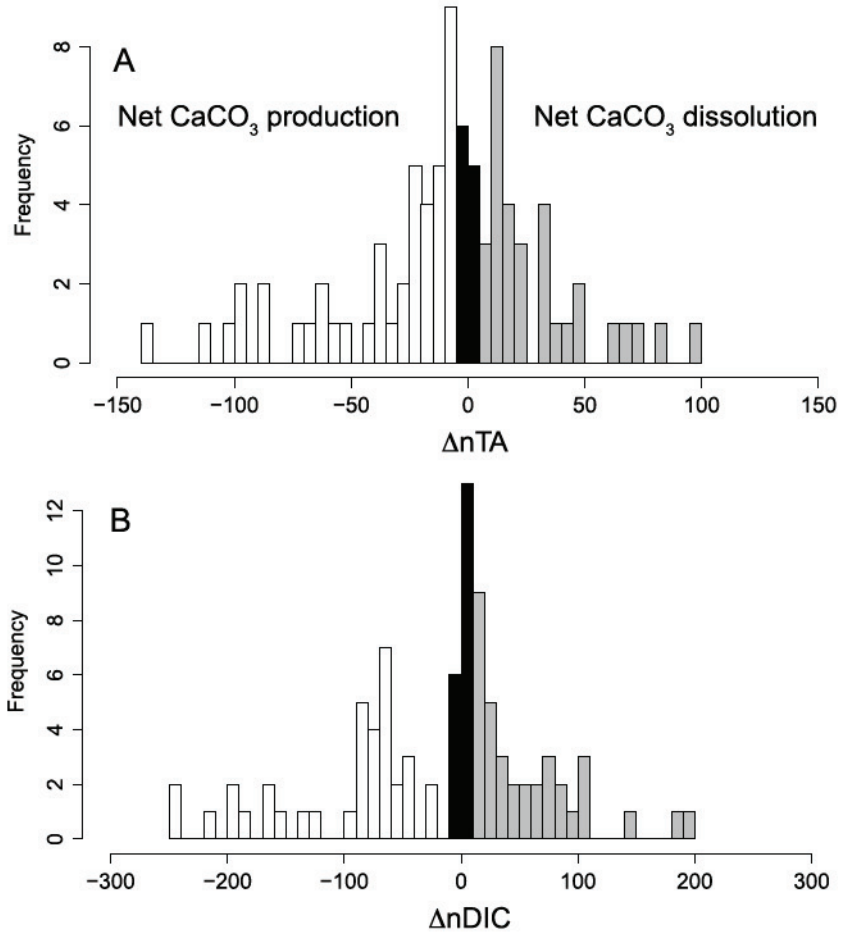

Figure 5. Histograms of (a) ΔnTA and (b) ΔnDIC. Deficits (white) and surpluses (dark gray) were significantly different from zero ($P<0.05$). The black bars denote the values that were not significantly different from zero.

measurements fell within the not significant band. For ΔnTA, 51% of the observations were significantly negative (deficits) compared to 36% of the observations that were significantly positive (surpluses). For ΔnDIC the observations were more evenly balanced with 42% significantly negative to 46% significantly positive.

Season had a significant effect on ΔnTA (ANOVA, $F(1,89) = 27.0$, $P < 0.0001$) and ΔnDIC (ANOVA, $F(1,81) = 101.1$, $P < 0.0001$) with the sign of ΔnTA and ΔnDIC, actually reversing on five of the seven transects (Figure 5). In order to look at whether the effects season varied from north to south or with distance from shore with sufficient statistical power to see significant differences the data were pooled into upper (Fowey-1 and Pennekamp-2), middle (Fiesta-3, Long-4, and Marathon-5), and lower (7 mile-6 and Looe-7) groups and into inner and outer groups. With the data broken out in this way it becomes striking how closely the spatial trends in ΔnTA with location (Figure 6a) and distance from shore (Figure 6c) parallel the spatial trends in ΔnDIC (Figures 6c and 6d). See Tables 1 and 2 for the results of the ANOVAs and post hoc mean tests performed to look at the effects of season, location, and distance alone and in combination on ΔnTA and ΔnDIC. Here we point out the strongest effect which was the interaction between season and distance from shore clearly seen in Figures 6c and 6d. The effect of season on ΔnTA was significant on the inner reefs ($dif = 100.0 \pm 12.4$ μmol kg^{-1}, $P < 0.0001$) but not the outer ($dif = 16.9 \pm 8.1$ μmol kg^{-1}, $P = 0.16$). Similarly, the difference in ΔnDIC on the inner reefs ($dif = 176.4 \pm 13.4$ μmol kg^{-1}, $P < 0.0001$) was highly significant but not on the outer reefs ($dif = 47.8 \pm 9.0$ μmol kg^{-1}, $P < 0.0001$).

3.2. Aragonite Saturation State (Ω_{ar})

Contour maps of Ω_{ar} for each of the cruises are shown in Figure 7. These maps show the broad-scale spatial trends in Ω_{ar} with elevated values on the inner reefs relative to the ocean during the spring and summer and

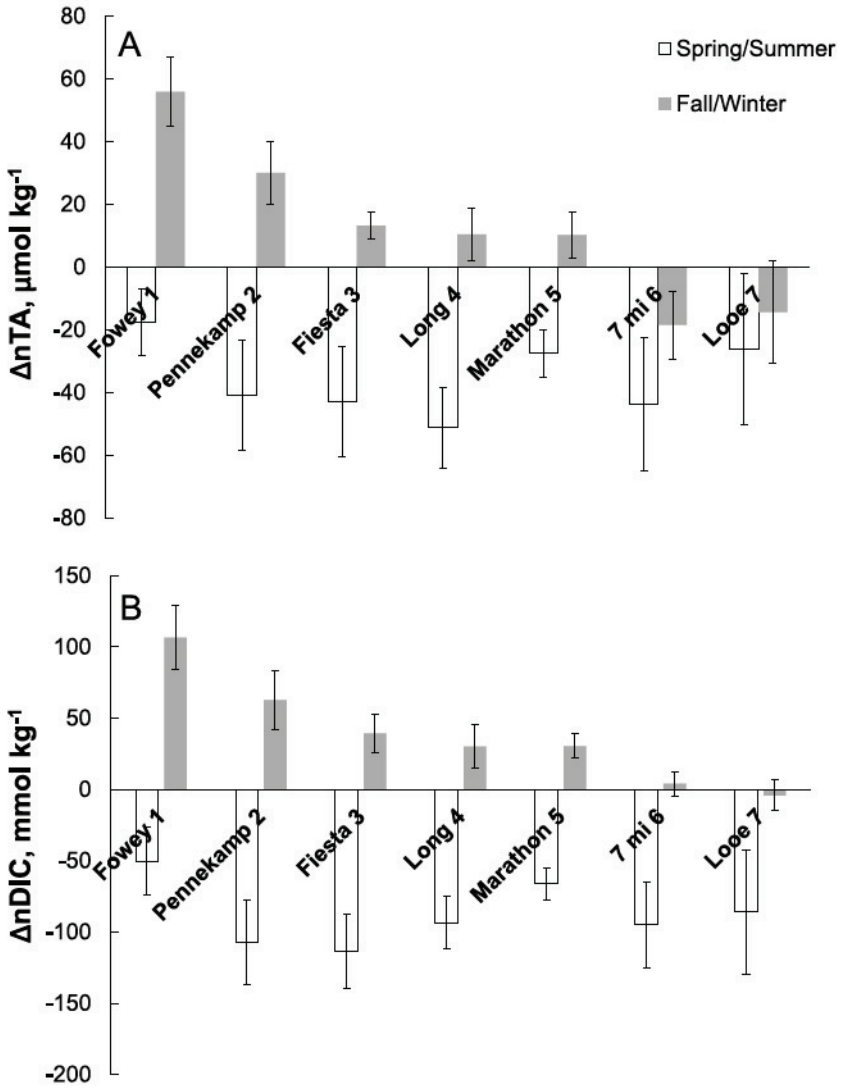

Figure 6. Seasonal changes in (a) Δ*n*TA and (b) Δ*n*DIC by transect line (ordered from north to south). The error bars are ±SEM.

depressed values during the fall and winter (note that there was considerable interannual variability). There was a highly significant interaction between season and distance from shore (Figure 8 and Table 1). During the winter the inner reefs 3.43 ± 0.07 were significantly lower than the outer reefs 3.75 ± 0.05 (Tukey's HSD, $P = 0.014$; Table 2). During the summer the trend was reversed but the differences were not significant, i.e., inner 3.70 ± 0.08 versus outer 3.58 ± 0.05.

3.3. *n*TA-*n*DIC Vector Analysis

*n*TA-*n*DIC plots are useful for getting a visual sense of the big picture of a data set before drilling down into the small details. *n*TA-*n*DIC plots for each cruise are shown in Figure 9. At a glance it can be seen that *n*TA and *n*DIC properties of the reefal water tend to fall along lines. The red symbol representing the properties of the offshore ocean water falls along that line and often but not always is positioned at one end of the line. This is visual support for the hypothesis that the red point represents the properties of the source for the reefal waters. The next important thing to note is that during the spring and summer most data points tend to fall to the left and down from the ocean point and during the fall and winter most points fall to right and up relative on the ocean point. Referring back to Figure 2, see how each TA-DIC diagram can be divided into four quadrants centered in the ocean end-member point. It can be seen that the data in Figure 9 fall mostly into the lower left (+NCC and +NCP) and upper right (−NCC and −NCP) quadrants. During the spring and summer

Table 1. Results of ANOVAs

DV	Source	*df*	*F* Ratio	*P*[a]
Δ*n*TA	location	2133	14.8	**<0.0001**
	distance	1133	25.5	**<0.0001**
	season	1133	61.8	**<0.0001**
	season × location	2133	3.5	0.24
	season × distance	1133	31.2	**<0.0001**
	location × distance	2133	10.2	**<0.0001**
	season × location × distance	2133	1.0	0.35
Δ*n*DIC	location	2138	6.9	**0.0014**
	distance	1138	16.4	**<0.0001**
	season	1138	193.4	**<0.0001**
	season × location	2138	3.4	**0.035**
	season × distance	1138	63.6	**<0.0001**
	location × distance	2138	6.1	**0.0028**
	season × location × distance	2138	1.0	0.44
Ω_{ar}	location	2143	1.8	0.16
	distance	1143	2.5	0.12
	season	1143	0.6	0.43
	season × location	2143	1.1	0.32
	season × distance	1143	11.6	**0.0009**
	location × distance	2143	0.6	0.55
	season × location × distance	2143	0.7	0.49
τ	location	224	0.6	0.54
	distance	124	2.2	0.15
	season	124	0.0	0.86
	season × location	224	0.8	0.45
	season × distance	124	2.8	0.11
	location × distance	224	0.4	0.65
	season × location × distance	224	0.0	0.99
NCC	location	278	10.4	**<0.0001**
	distance	178	0.5	0.5
	season	178	29.4	**<0.0001**
	season × location	278	0.8	0.44
	season × distance	178	7.6	**0.007**
	location × distance	278	1.6	0.22
	season × location × distance	278	1.3	0.27
NCP	location	277	2.0	0.15
	distance	177	0.3	0.58
	season	177	128.8	**<0.0001**
	season × location	277	3.5	**0.034**
	season × distance	177	5.9	**0.017**
	location × distance	277	0.9	0.43
	season × location × distance	277	2.5	0.09

[a]Significant results ($p < 0.05$) are shown in bold.

the geochemical data are telling us that the reefal communities are net producers of organic (+NCP) and inorganic carbon (+NCC) because the data points are falling into the lower left quadrant. However, during the fall and winter, most but not all of the sampled reefs are undergoing net dissolution (−NCC) and net respiration (−NCP) because the data points are falling to the upper right quadrant. It is interesting that we did not sample any reefs where NCC was positive and NCP was negative or vice versa (NCC negative and NCP positive). It is as if these states are not allowed for some physical, chemical, or biological reason.

If we turn next to the slopes of *n*TA-*n*DIC relationship for each cruise we can make inferences about the relative rates of NCC and NCP on a reefal tract-wide basis. Recall from Figure 2 that if data points fall along a line with a slope close to 0, then we know that the production/respiration of organic matter is the dominant biogeochemical process altering the carbonate chemistry of the water. On the other hand, if the line described by the data points is 2.0 we know that production/dissolution of $CaCO_3$ is the dominant process. If the slope of the line is 1.0, then we know that the rates of organic and inorganic carbon production or destruction are equal. Slopes were determined for each of the cruise data sets by linear regression, and the information is summarized in Table 3. All of the regressions were highly significant ($P < 0.0001$). Slopes ranged from a low of 0.43 to a high of 1.18 (Table 3, column 5). Using equation (3), NCC:NCP ratios were computed from the each of the slopes (Table 3, column 8). NCC:NCP ranged from a low of 0.27 to a high of 1.44. Change in the relative balance between NCC and NCP is important because it influences how community metabolism alters the Ω_{ar} of the water (Figure 2). When NCC:NCP is <1 drawdown of *n*TA and *n*DIC results in an elevation of Ω_{ar} relative to ocean source water when rates of NCC and NCP are positive. An example of this is most clearly seen in the two spring cruises (Figure 4). The average elevation in Ω_{ar} was 0.12 units in 09 April and 0.18 units in 10 May (Table 3, column 9). When NCC and NCP are negative a slope <1 results in a depression of Ω_{ar}. Examples of this are the 09 and 10 December cruises (Figure 4), where Ω_{ar} was depressed by −0.09 and −0.17 units (Table 3, column 9). When the slope of the *n*TA-*n*DIC data is >1 the impact on the carbonate chemistry is reversed. Example of this is the August 09 cruise when +NCC and +NCP resulted in the depression of Ω_{ar} by −0.06 units and in 09 October when a slope >1 resulted in the elevation of Ω_{ar} by 0.15 units.

Table 2. Post Hoc Mean Tests

DV	Factor 1	Factor 2	Mean	SE	Connecting Letter
ΔnTA	Season	Distance	μmol kg^{-1}		
	Winter	Inner	14.8	8.3	A
		Outer	10.8	5.5	A
	Summer	Inner	−85.2	9.3	B
		Outer	−6.1	6.0	A
	Season	Location	μmol kg^{-1}		
	Winter	Lower	−17.3	9.8	A
		Middle	12.4	7.4	A, B
		Upper	43.8	8.4	B, C
	Summer	Lower	−73.0	9.7	D
		Middle	−32.7	8.3	C
		Upper	−31.3	10.6	C
ΔnDIC	Season	Distance	μmol kg^{-1}		
	Winter	Inner	50.3	8.8	A
		Outer	18.7	6.1	A
	Summer	Inner	−126.0	10.0	B
		Outer	−29.1	6.7	A
	Season	Location	μmol kg^{-1}		
	Winter	Lower	3.1	10.9	A
		Middle	32.3	8.3	A
		Upper	68.2	8.4	B
	Summer	Lower	−84.4	10.8	C
		Middle	−75.7	9.3	C
		Upper	−72.5	11.0	C
Ω_{ar}	Season	Distance			
	Winter	Inner	3.43	0.07	A
		Outer	3.75	0.05	B
	Summer	Inner	3.70	0.08	A, B
		Outer	3.58	0.05	A, B
τ	Season	Distance	days		
	Winter	Inner	6.0	0.8	A
		Outer	6.1	1.0	A
	Summer	Inner	7.4	1.2	A
		Outer	4.3	0.9	A
	Season	Location	days		
	Winter	Lower	6.0	1.3	A
		Middle	6.2	0.9	A
		Upper	6.0	1.1	A
	Summer	Lower	6.8	1.5	A
		Middle	4.8	1.1	A
		Upper	6.5	1.3	A
NCP	Season		mmol C m^{-2} d^{-1}		
	Winter		−32.0	5.4	A
	Summer		61.8	6.2	B
	Season	Location	mmol C m^{-2} d^{-1}		
	Winter	Lower	−12.4	10.4	B
		Middle	−27.5	7.9	B, C
		Upper	−56.1	9.8	C
	Summer	Lower	50.9	10.5	A
		Middle	71.9	9.8	A
		Upper	62.6	11.9	A
	Season	Distance	mmol C m^{-2} d^{-1}		
	Winter	Inner	−44.3	7.8	A
		Outer	−19.6	7.6	A
	Summer	Inner	69.6	8.8	B
		Outer	54.0	8.8	C

Table 2. (continued)

DV	Factor 1	Factor 2	Mean	SE	Connecting Letter
NCC	Season		mmol $CaCO_3$ m^{-2} d^{-1}		
	Winter		−6.6	3.6	A
	Summer		23.4	4.2	B
	Location		mmol $CaCO_3$ m^{-2} d^{-1}		
	Lower		25.5	5.0	A
	Middle		6.6	4.2	B
	Upper		−6.9	5.2	B
	Season	Location	mmol $CaCO_3$ m^{-2} d^{-1}		
	Winter	Lower	13.4	7.0	A, B
		Middle	−6.1	5.2	B, C
		Upper	−27.2	6.5	C
	Summer	Lower	37.5	7.0	A
		Middle	19.2	6.5	A
		Upper	13.4	7.0	A, B
	Season	Distance	mmol $CaCO_3$ m^{-2} d^{-1}		
	Winter	Inner	−12.4	5.2	C
		Outer	−0.8	5.1	B, C
	Summer	Inner	32.9	5.9	A
		Outer	13.9	5.9	A, B

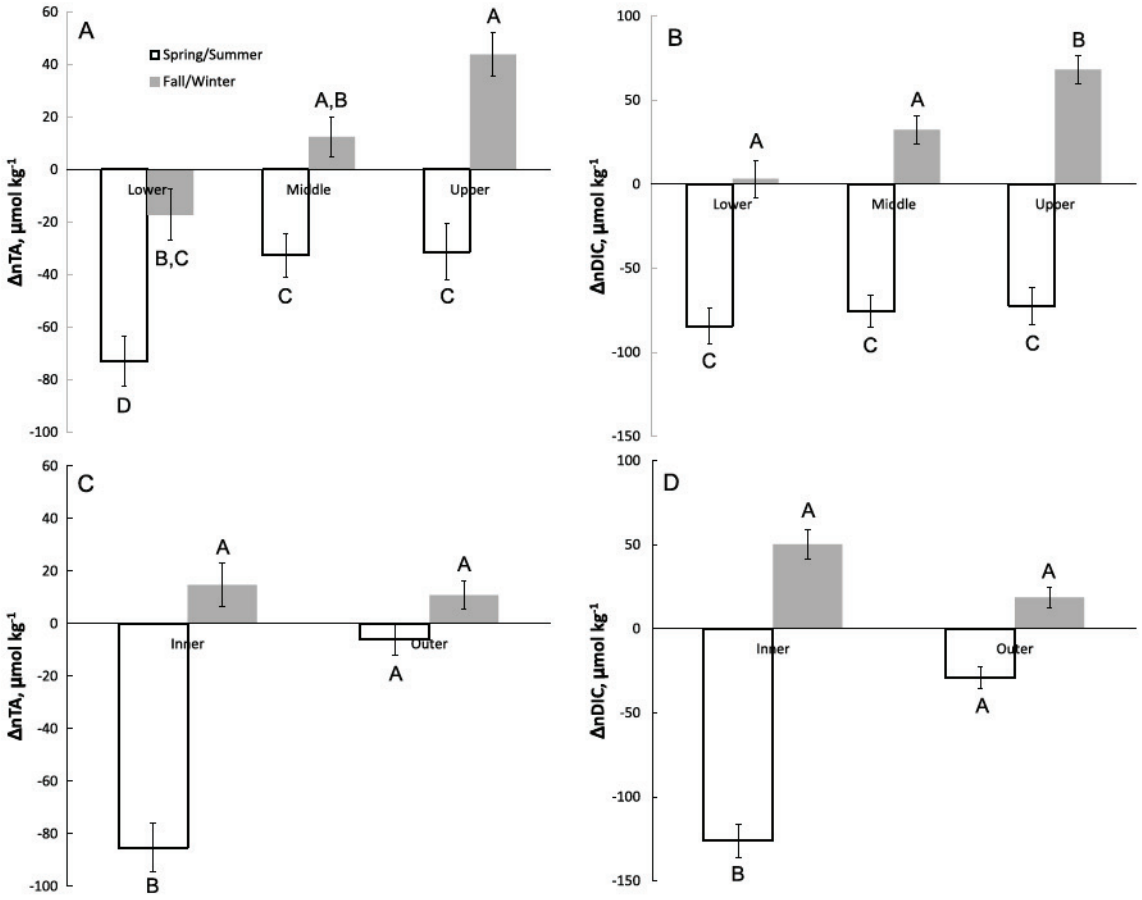

Figure 7. Seasonal and spatial trends in Δ*n*TA and Δ*n*DIC by (a and b) location and by (c and d) distance from shore. The dissimilar letters indicate the means that were significantly different ($P < 0.05$).

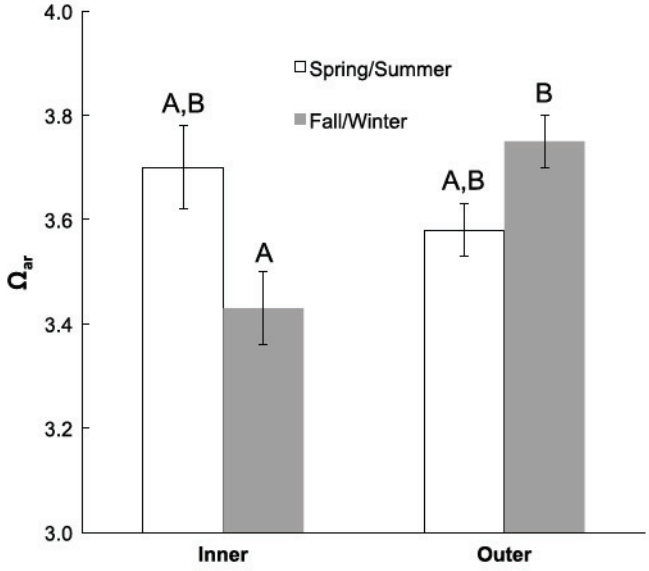

Figure 8. Seasonal changes in Ω_{ar} by distance from shore. The error bars are ±SEM.

The analysis above was based on the aggregated data for each cruise. Breaking the data out by location (upper = transects 1 and 2; middle = transects 3, 4, and 5; and lower = transects 6 and 7), distance from shore (inner <1.5 km and outer >1.5 km), and by season (spring/summer = April, May, and August and fall/winter = October, November, and December) was helpful in revealing interesting temporal and spatial trends at the regional level. Slopes were quite low in the upper and middle Florida Keys (0.46 ± 0.06 and 0.51 ± 0.07) indicating NCC:NCP ratios of 0.30 ± 0.04 to 0.34 ± 0.05, meaning that organic carbon production was 3 times inorganic carbon production. In the lower Florida Keys the slope was 0.96 ± 0.13 indicative of a NCC:NCP ratio of 0.92 ± 0.13 (Table 3, middle section). The outcome of the dominance of photosynthetic activity in the upper and middle Florida Keys was an elevation in Ω_{ar} of 0.26–0.32 units, while in the lower Florida Keys despite a large drawdown in *n*TA and *n*DIC Ω_{ar} barely changed (i.e., −0.01 units). During the fall/winter the vectors in the upper and middle Florida Keys were reversed (i.e., directed into the upper right quadrant) with slightly reduced magnitudes (l) of 30.0 to 67.1 μmol kg^{-1}. The slopes were still low (0.56 ± 0.09 and 0.45 ± 0.09), indicating that respiration exceeded dissolution by a factor of 2. The result of this biogeochemical activity was a depression of Ω_{ar} by 0.15 to 0.24 units. In the lower Florida Keys the vector was directed into the lower right quadrant (−NCP and +NCP). The slope of 1.28 ± 0.31 indicated that the NCC:NCP was 1.78 ± 0.43 and the change in Ω_{ar} was −0.03 units.

Breaking the data out by season and distance from shore also revealed interesting trends (Table 3, bottom section). The inner reefs displayed the greatest drawdown in *n*TA and *n*DIC. The magnitude of the metabolic vector was 150.9 μmol kg^{-1} and the slope was 0.84 ± 0.18, indicating a NCC:NCP ratio of 0.72 ± 0.16. The result of the excess of photosynthesis over calcification was an elevation in Ω_{ar} of 0.11 units. The drawdown of *n*TA and *n*DIC on the outer reefs was smaller, resulting in a vector with a magnitude of 30 μmol kg^{-1}. However, because the slope was much lower (0.42 ± 0.07) indicating a NCC:NCP ratio of 0.27 ± 0.04, the impact on Ω_{ar} was bigger, i.e., +0.17 units. During the fall/winter both vectors were directed into the upper right quadrant. The magnitude of the vector for the inner reefs was greater than for the outer reefs (62.9 versus 29.1 μmol kg^{-1}), and the slopes (0.78 ± 0.09 versus 0.63 ± 0.10) indicated that the NCC:NCP ratios were 0.46 to 0.64. Under these conditions the excess of respiration over dissolution acidifies the water and lowers Ω_{ar} 0.08 units.

3.4. Residence Time

Residence times broken down by season, location, and distance from shore are shown in Figure 10 and summarized in Table 2. The biggest range was during the summer when it varied from 7.4 days on the inner reefs to 4.3 days on the outer reefs. However, ANOVA showed that difference and the others shown in Figure 10 were not statistically significant (Table 1). The average residence time over the 20 month study was 5.6 ± 1.7 days. For the purposes of computing NCC and NCP the actual measured value of τ at each station was used in the calculation. If τ was not measured at a specific location the value from the closest station was used.

3.5. Net Ecosystem Calcification (NCC) and Net Community Production (NCP)

Rates of NCC and NCP were computed from the ΔnTA, ΔnDIC, and residence time data using equations (1) and (2). Figure 11 shows the data for each reefal line ordered from north to south. The most salient features of the data are that during the spring/summer, rates of NCC are positive and fairly uniform across the FRT ranging from 12.5 to 23.5 mmol m^{-2} d^{-1}. However, during the fall/winter there was a gradient

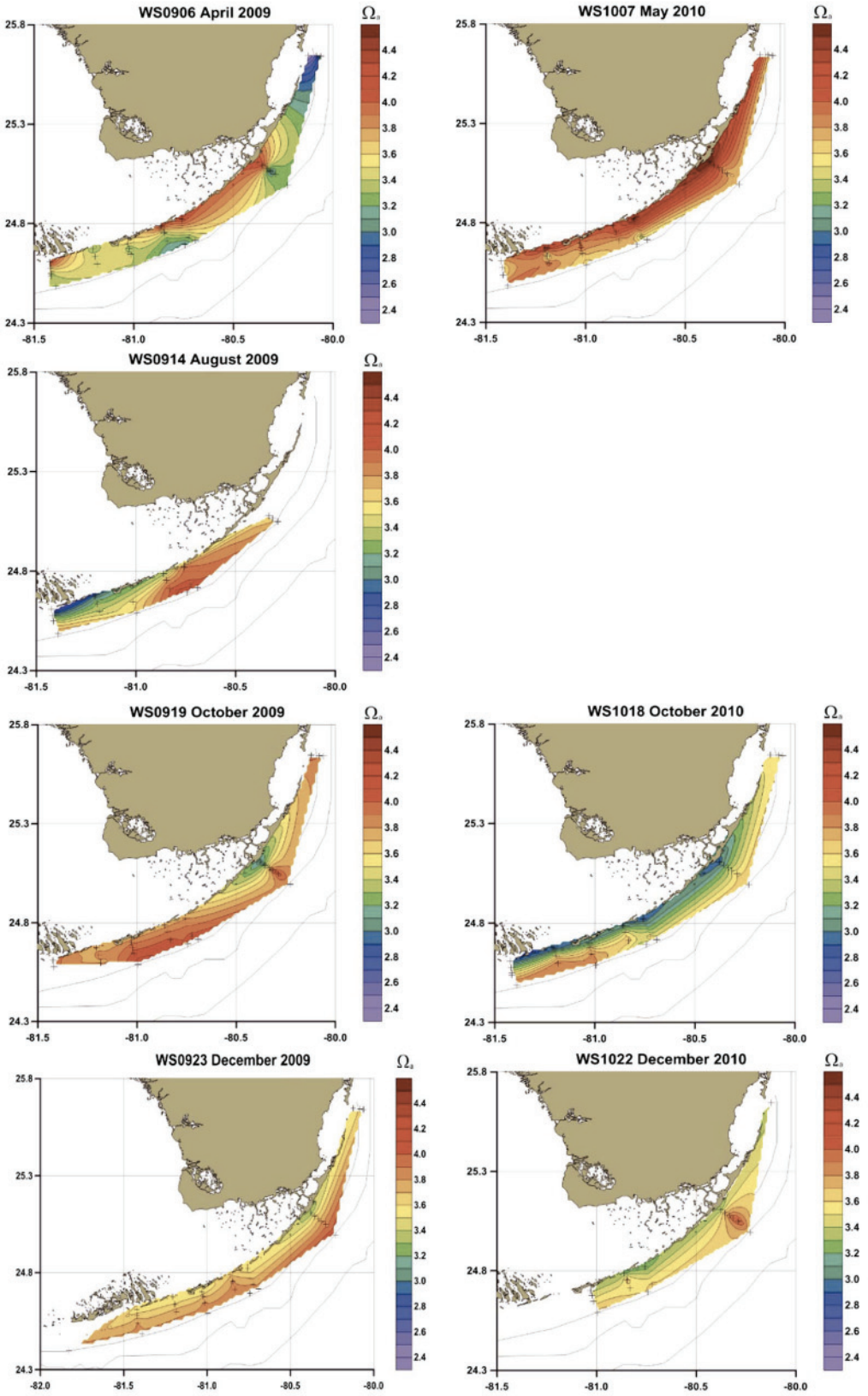

Figure 9. Contour maps of Ω_{ar} by season.

Table 3. Metabolic Vector Characteristics and Computed NCC:NCP Ratios and $\Delta\Omega_{ar}$[a]

Date		ΔnTA (μmol kg^{-1})	ΔnDIC	L[b]	m[c]	r^2	P	NCC:NCP[d]	$\Delta\Omega_{ar}$[e]
09 Apr		−22.9 ± 6.2	−13.8 ± 10.8	26.7	0.49 ± 0.06	0.72	<0.0001	0.32 ± 0.04	0.12
09 Aug		−26.0 ± 25.1	−26.4 ± 19.6	37.1	1.18 ± 0.10	0.88	<0.0001	1.44 ± 0.12	−0.06
09 Oct		18.3 ± 10.3	54.9 ± 11.6	95.6	1.16 ± 0.11	0.79	<0.0001	1.38 ± 0.13	0.15
09 Dec		−2.8 ± 3.0	17.1 ± 4.7	17.3	0.43 ± 0.10	0.40	0.0002	0.27 ± 0.06	−0.09
10 May		−19.1 ± 7.9	−48.9 ± 12.9	52.5	0.57 ± 0.05	0.85	<0.0001	0.40 ± 0.03	0.18
10 Oct		18.3 ± 10.3	54.9 ± 11.6	57.9	0.82 ± 0.09	0.76	<0.0001	0.69 ± 0.07	−0.05
10 Dec		22.3 ± 5.9	31.9 ± 10.2	38.9	0.50 ± 0.09	0.67	<0.0001	0.33 ± 0.06	−0.17
Location	Season								
U	S	−22.1 ± 11.8	−60.0 ± 13.3	63.9	0.46 ± 0.06	0.77	<0.0001	0.30 ± 0.04	0.32
M	S	−20.5 ± 9.2	−57.9 ± 10.6	61.4	0.51 ± 0.07	0.66	<0.0001	0.34 ± 0.05	0.26
L	S	−45.8 ± 10.9	−57.9 ± 12.6	73.8	0.96 ± 0.13	0.75	<0.0001	0.92 ± 0.13	−0.01
U	W	34.4 ± 8.2	57.6 ± 10.3	67.1	0.56 ± 0.09	0.61	<0.0001	0.39 ± 0.06	−0.24
M	W	12.7 ± 8.2	27.2 ± 9.5	30.0	0.45 ± 0.09	0.42	<0.0001	0.29 ± 0.06	−0.16
L	W	−11.1 ± 11.2	4.6 ± 12.9	12.0	1.28 ± 0.31	0.48	0.0007	1.78 ± 0.43	−0.03
Distance	Season								
Inner	S	−84.3 ± 10.1	−125.2 ± 10.7	150.9	0.84 ± 0.18	0.54	0.0002	0.72 ± 0.16	0.11
Outer	S	−5.7 ± 6.5	−29.5 ± 7.0	30.0	0.42 ± 0.07	0.47	<0.0001	0.27 ± 0.04	0.17
Inner	W	18.6 ± 9.1	60.1 ± 9.2	62.9	0.78 ± 0.09	0.74	<0.0001	0.64 ± 0.07	−0.08
Outer	W	21.1 ± 5.9	20.1 ± 6.3	29.1	0.63 ± 0.10	0.41	<0.0001	0.46 ± 0.07	−0.08

[a]Mean metabolic vectors were determined for each cruise and for groups of stations broken out by location and season or distance from shore and season and resolved into their component *Dn*TA and *Dn*DIC vectors (mean ± SEM).
[b]Magnitude was computed $\sqrt{(DnTA^2 + DnDIC^2)}$.
[c]Results of linear regression of *n*TA-*n*DIC data points, slope *m*, adjusted r^2, and significance level *P*.
[d]NCC:NCP ratio computed using equation (3) (mean ± SEM).
[e]$\Delta\Omega_{ar}$ computed using equation (4).

inNCC with strongly negative rates (dissolution) at Fowey in the north (−42.7 mmol m^{-2} d^{-1}), moderate negative rates throughout the middle Florida Keys (−6.5 to −10.9 mmol m^{-2} d^{-1}), and reduced but still positive rates (calcification) of NCC at the two most southerly reefs (4.2 to 6.7 mmol m^{-2} d^{-1}). Similarly, rates of NCP are positive and uniform across the FRT in the spring/summer (46.2–89.3 mmol m^{-2} d^{-1}). During the fall/winter rates of NCP became negative (respiration) with the most northerly reef (Fowey) standing out as having the most negative rate (−107.3 mmol m^{-2} d^{-1}) and the rest of the reefs falling between (−7.9 and −33.7 mmol m^{-2} d^{-1}).

3.5.1. NCC

Seasonal trends in NCC broken out by location (upper, middle, and lower Florida Keys) or distance from shore are shown Figures 12a and 12c. Season and location and an interaction between season and distance from shore were found to have significant effects on NCC (Table 1). The specific means that were found to be different by Tukey's post hoc comparison are given in Table 2.

3.5.2. NCP

Seasonal trends in NCP broken out by location or distance from shore are shown in Figures 12b and 12d. Season and interactions between season and location or season and distance from shore were found to have significant effects on NCP (Table 1). The specific means that were found to be different by Tukey's post hoc comparison are given in Table 2.

3.5.3. Annual Rates of NCC and NCP

Rates of annual NCC on each of the reefal lines ordered from north to south are shown in Figure 13a. Rates ranged from −1.1 ± 0.4 to 1.0 ± 0.3 kg $CaCO_3$ m^{-2} yr^{-1}. If the negative rate at Fowey is included, the average across the FRT is not significantly different from zero (0.29 ± 0.26 kg $CaCO_3$ m^{-2} yr^{-1}, one-sided *t* test, $T(6) = 1.15$, $P = 0.15$). If the data point for Fowey-1 is excluded (as a potential outlier), then the average annual NCC for the FRT is significantly greater than zero (0.53 ± 0.13 kg $CaCO_3$ m^{-2} yr^{-1}, one-sided *t* test, $T(5) = 4.19$, $P = 0.004$). Of the seven reefal lines only Long Key-4 (0.67 ± 0.24 kg $CaCO_3$ m^{-2} yr^{-1}, one-sided *t* test, $T(5) = 2.91$, $P = 0.017$) and 7 mile-6 (0.97 ± 0.28 kg $CaCO_3$ m^{-2} yr^{-1}, one-sided *t* test, $T(5) = 3.60$, $P = 0.008$) had annual NCC rates significantly greater than zero, while the rate at Fowey-1 (−1.10 ± 0.37 kg $CaCO_3$ m^{-2} yr^{-1}, one-sided *t* test, $T(4) = 2.98$, $P = 0.048$) was significantly less than zero. The annual rates of NCP are shown in Figure 13b. If the negative rate at Fowey-1 is included the average across the FRT was 10.1 ± 4.5 mol C m^{-2} yr^{-1} (one-sided *t* test, $T(6) = 2.2$, $P = 0.034$). If the data point for Fowey-1 is excluded,

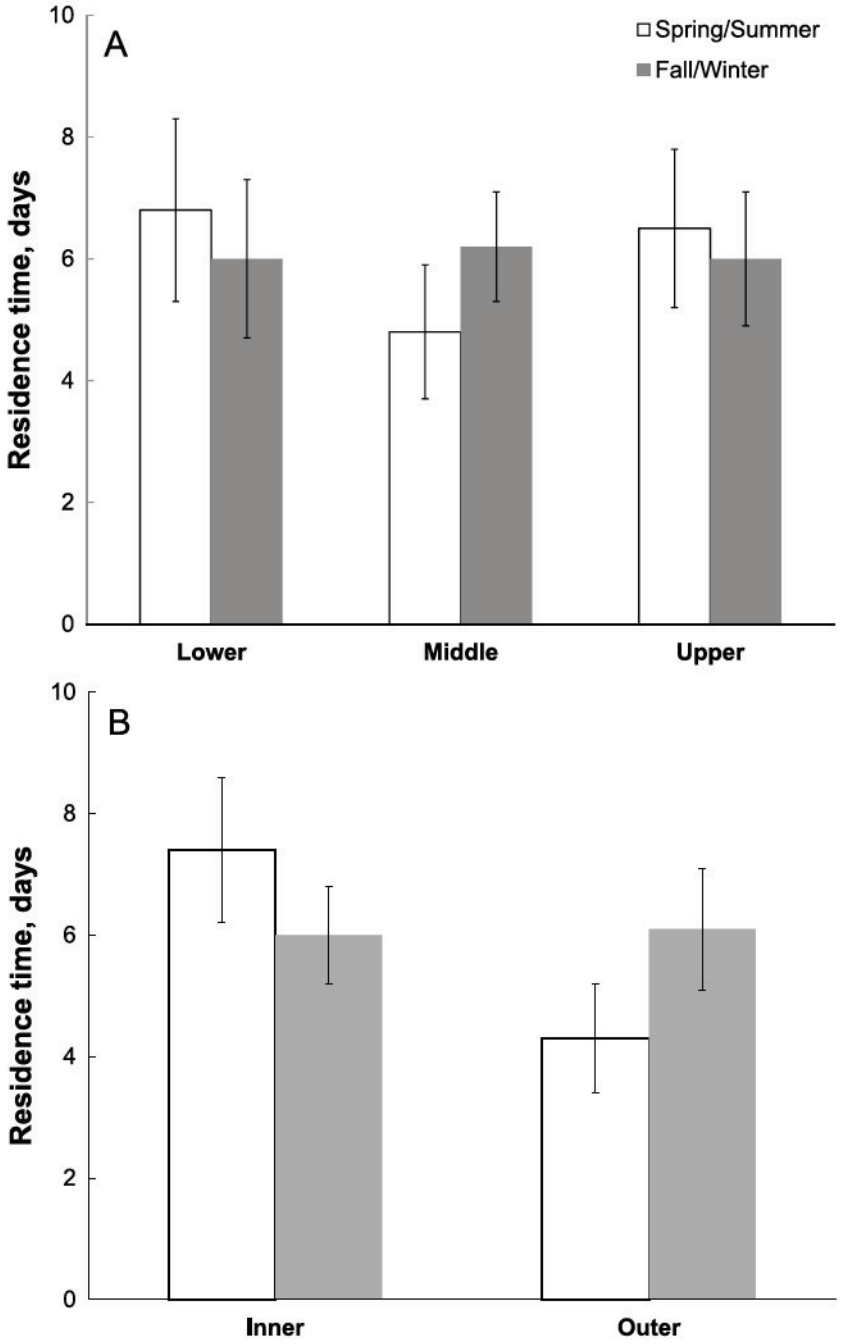

Figure 10. Seasonal differences in water residence time by (a) location and by (b) distance from shore. The error bars are ±SEM. There were no significant differences.

then the average annual NCP for the FRT is 14.4 ± 1.5 mol C m^{-2} yr^{-1} (one-sided t test, $T(5) = 9.3$, $P = 0.0001$). Of the seven reefal lines only Fiesta Key-3 (20.9 ± 5.7 mol C m^{-2} yr^{-1}, one-sided t test, $T(5) = 2.7$, $P = 0.028$) and Long Key-4 (6.1 ± 0.28 mol C m^{-2} yr^{-1} one-sided t test, $T(5) = 2.7$, $P = 0.022$) had annual NCP rates significantly greater than zero. The NCP rate at Fowey-1 (-15.9 ± 14.0 mol C m^{-2} yr^{-1}, one-sided t test, $T(3) = -1.0$, $P = 0.2$) was not significantly less than zero.

3.6. Relationship Between NCC and Ω_{ar} and Between NCC and NCP

A linear regression found that Ω_{ar} explained a significant amount of the observed variance in NCC, adjusted $r^2 = 0.21$, RMSE = 15.8, $F(1,27) = 8.3$, $P = 0.008$ (Figure 14a). The best fit equation was NCC = $-67.6 + 19.0 \times \Omega_{ar}$.

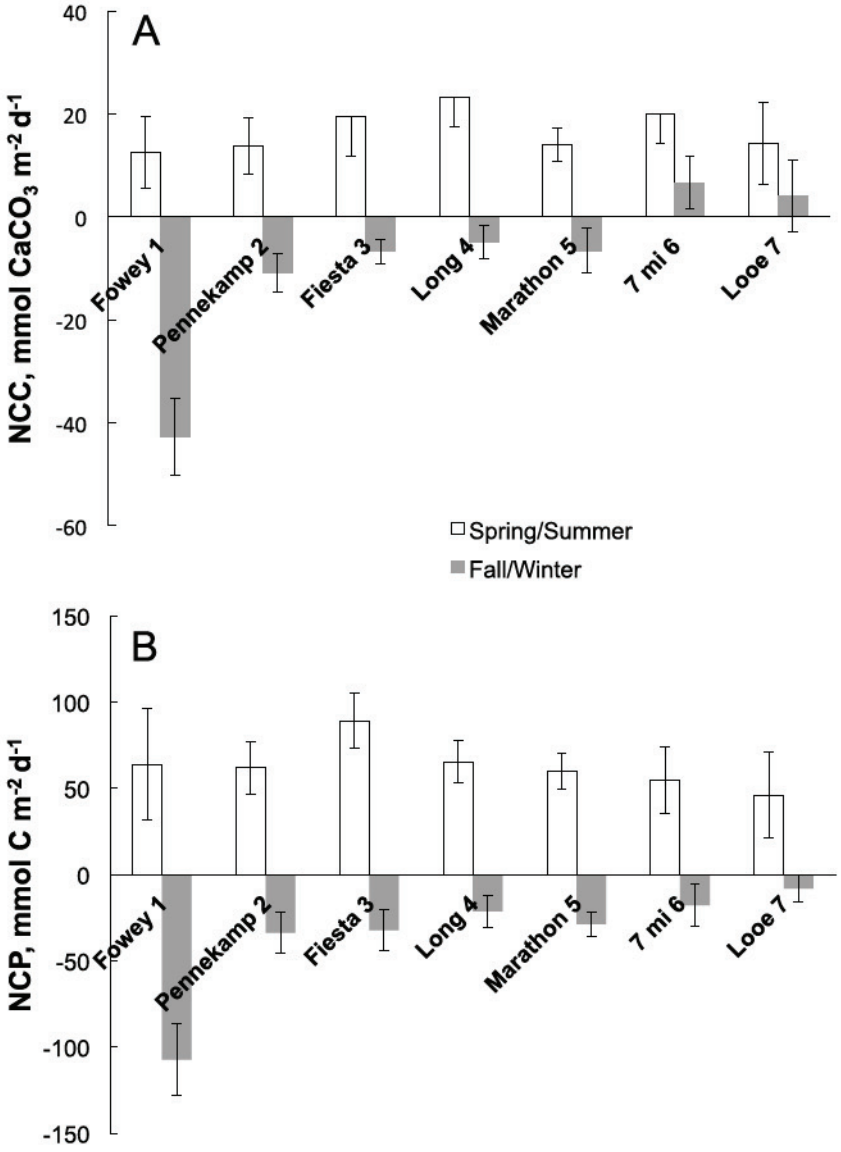

Figure 11. Seasonal and spatial trends in NCC and NCP by transect line.

Both the intercept (-67.6 ± 23.6, $P = 0.0086$) and the slope (19.0 ± 6.6, $P = 0.0077$) were significantly different from zero. The x intercept of the line or the threshold Ω_{ar} where NCC = 0 was 3.6 ± 1.8. A linear regression revealed that NCP explained a larger relative proportion of the variance in NCC but not in terms of the absolute variance, adjusted $r^2 = 0.53$, RMSE = 15.0, $F(1,30) = 35.8$, $P < 0.0001$ (Figure 14b). The best fit equation was NCC = $0.0002 + 0.29 \times$ NCP. The intercept was not significantly different from zero (0.0002 ± 2.7, $P = 1$, ns) but the slope was (0.29 ± 0.05, $P < 0.0001$). Linear regression showed that Ω_{ar} and NCP were significantly correlated (adjusted $r^2 = 0.46$, $P < 0.0001$) and the best fit equation was $\Omega_{ar} = 3.65 + 0.0052 \times$ NCP (Figure S1 in the supporting information).

3.7. Sources of Error in the Measurements of NCC and NCP

The sign and magnitude of NCC are taken from the ΔnTA term in equation (1). Whether or not a measurement of ΔnTA is indicative of calcium carbonate formation or dissolution that is significantly different from zero was determined by performing t tests as described in section 3.3. If the mean nTA of the reefal water is significantly less than the ocean water, then the deficit of nTA indicates that a statistically significant amount of net carbonate has been formed. Similarly, if the mean nTA of the reefal water is significantly greater than the ocean water, then the surplus of nTA indicates that a statistically significant amount of

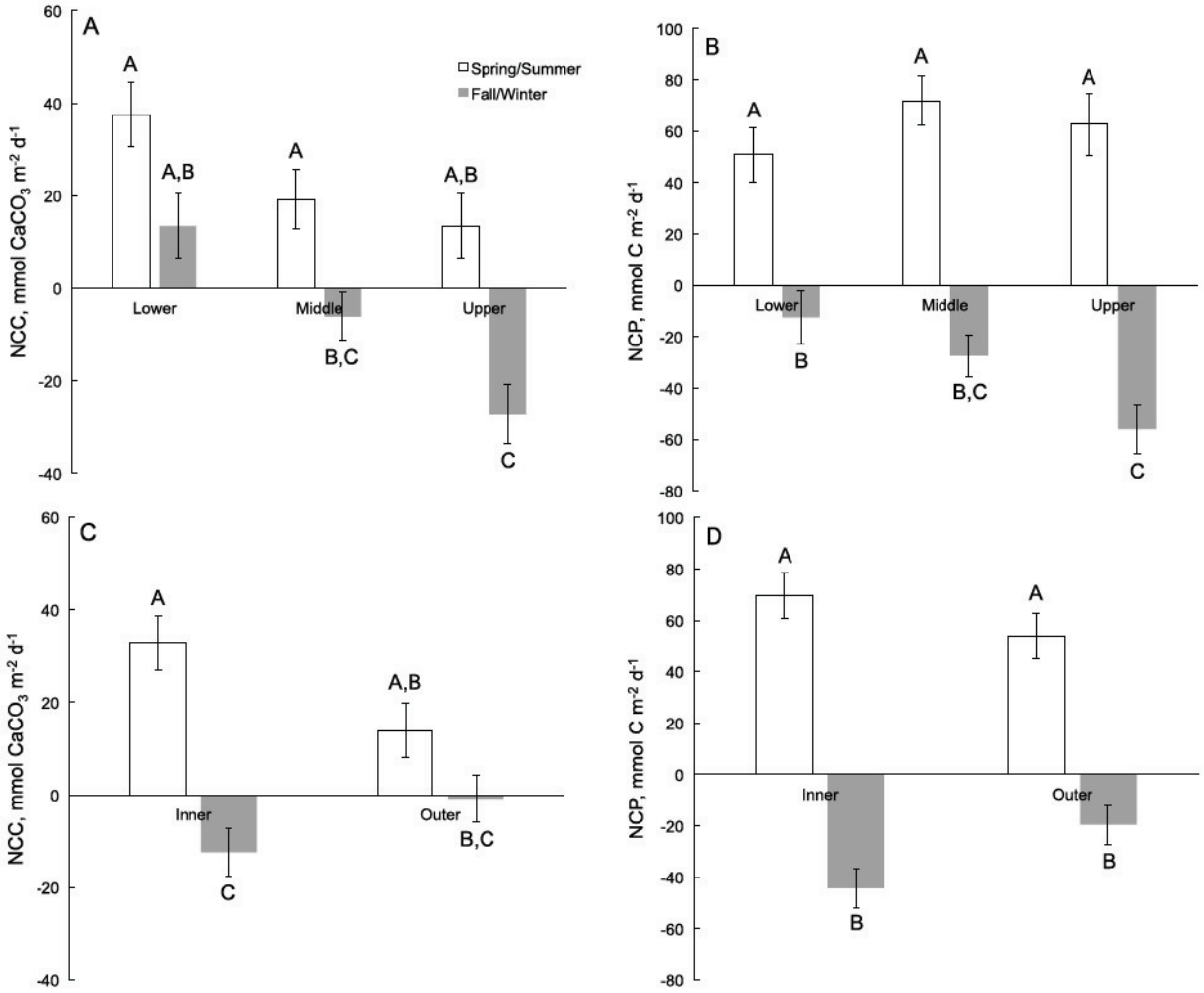

Figure 12. Seasonal and spatial trends in NCC and NCP by (a and b) location and by (c and d) distance from shore.

net carbonate has dissolved. As explained in section 3.3, ΔnTA values equaling or exceeding 5.2 μmol kg^{-1} meet this test. During the spring and summer cruises 63% of the ΔnTAs were less than −5.2, indicating statistically significant formation of $CaCO_3$, and 19% exceeded +5.2, indicating statistically significant dissolution. The average nTA depletion from the water column due to net calcification was 42 μmol kg^{-1} (±14% analytical uncertainty). During the fall and winter cruises the situation was reversed; 61% of the ΔnTAs exceeded +5.2 indicating significant dissolution while 22% were less than −5.2 indicating significant $CaCO_3$ formation. Average carbonate dissolution was 34 μmol kg^{-1} (±17% analytical uncertainty).

Converting this mass balance into production or dissolution rates involves multiplying by the factor (h/τ) in equation (1). Uncertainty in depth and residence time contributes to uncertainty in rates of NCC and NCP on a relative basis because they are multipliers and divisors in equations (1) and (2). In other words, the relative uncertainty in NCC or NCP contributed by uncertainty in h and τ is given by $\sqrt{[(\sigma_h/h)^2+(\sigma_\tau/_t)^2]}$, where σ_h is the standard error of depth and σ_τ is the standard error of residence time (τ). The standard error of station depths where NCC and NCP were measured averaged 1 m, and the average depth was 6 m so the relative uncertainty contributed by the depth term was 0.17. Uncertainty in residence time measurements is given in Table S2. On a relative basis the error averages ±39%. In a similar study performed in Bermuda the relative error in residence time averaged ±35% [*Venti et al.*, 2012]. Therefore, we believe that ±35–39% is a robust estimate of the error in residence time based on the Be-7 method. The relative uncertainty in NCC and NCP contributed by depth and residence time is $\sqrt{[(0.17)^2+(0.39)^2]}=0.42$ or 42%.

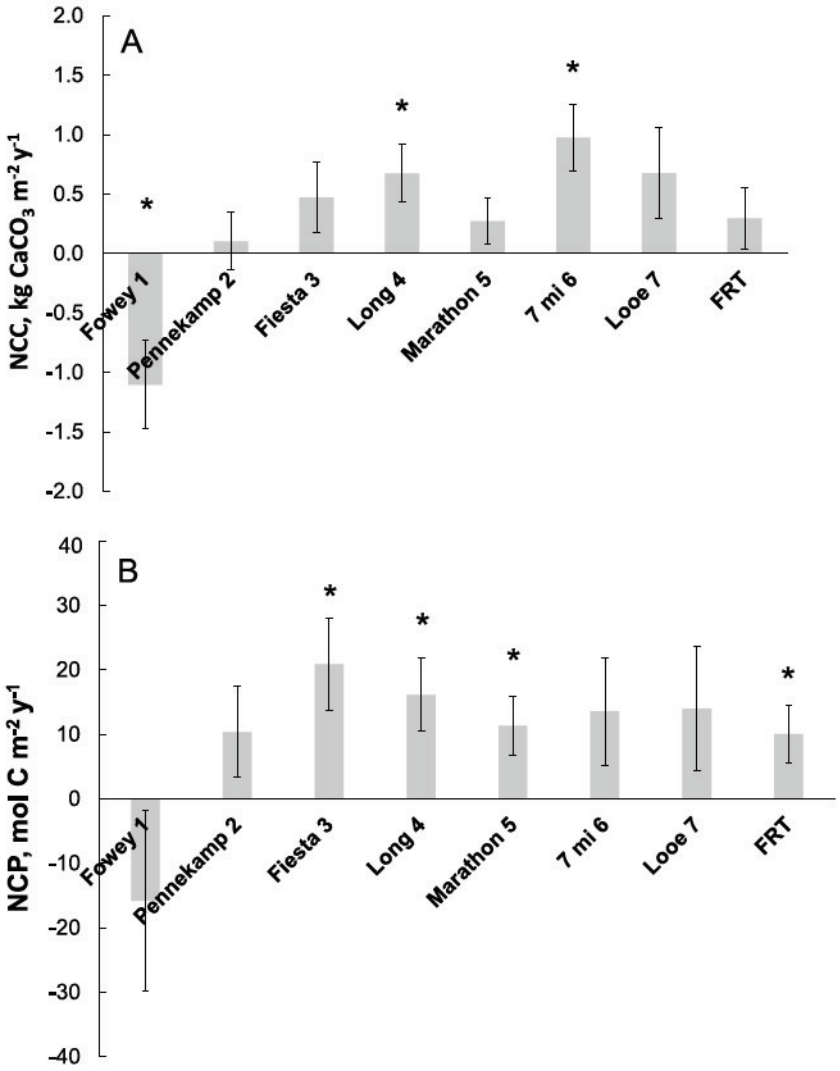

Figure 13. Annual rates of (a) NCC and (b) NCP across the FRT. The asterisks denote the rates significantly different from zero ($P < 0.05$).

The upshot of the error analysis is that we can say with an absolute uncertainty of ±5.2 μmol kg^{-1} that a specified amount of $CaCO_3$ has been formed or dissolved at a particular reefal location. Converting that absolute amount of carbonate production or dissolution to a rate introduces an additional relative uncertainty of ±40%. It is therefore important to keep in mind that we can know the amount of carbonate production/dissolution to a fairly high precision but the rate to a lesser precision.

4. Discussion

4.1. Historical Perspective and Comparison With the Broader Caribbean

The region-wide decline in live coral cover in the Caribbean from 50% in the 1970s to ~10% in the year 2000 has been well documented [*Gardner et al.*, 2003]. In the late 1970s white band disease caused massive population declines in two dominant Caribbean shallow-water species, *Acropora palmata* and *Acropora cervicornis* [*Gladfelter*, 1982]. This was followed by a second disease epidemic in the early 1980s that affected the long-spined sea urchin *Diadema antillarum* drastically reducing the numbers of the keystone herbivore, resulting in overgrowth of many reefs by seaweeds [*Cubit et al.*, 1984]. In the 1990s, *Gardner et al.* [2003] noted that the rate of decline of corals had greatly decreased and that some subregions including Florida and particularly Jamaica were showing signs of recovery. Despite that encouraging observation, studies in the Florida Keys conducted between 1996 and 2012 have documented the significant loss of colonies of the species

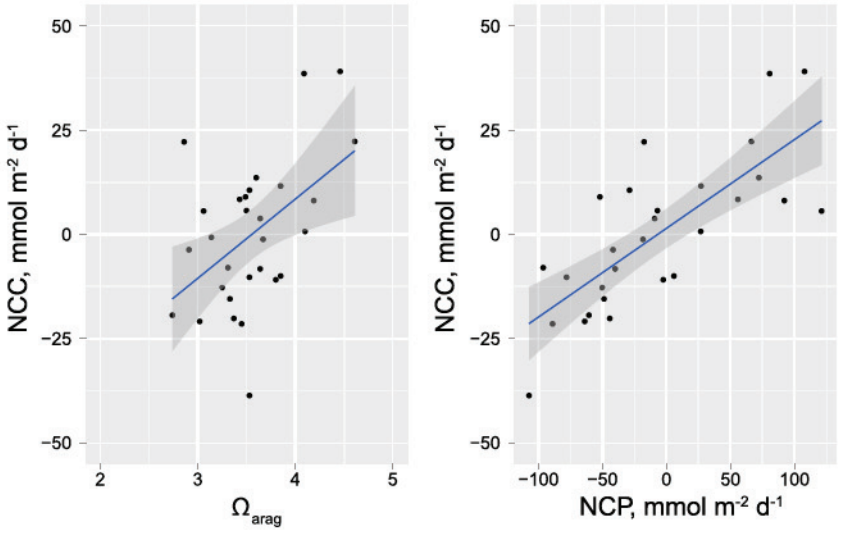

Figure 14. Relationships between (a) NCC and Ω_{ar} and (b) NCC and NCP. The blue line denotes the best fit linear regression. The gray shaded area denotes the 95% confidence interval.

Orbicella faveolata and the stasis of many other subdominant species (*Siderastrea* spp., *Montastraea cavernosa*, *Agaricia* spp., and *Porites astreoides*) with the net result that the live coral cover has further declined from 13% in 1996 to 8% in 2009 [*Vega-Rodriguez et al.*, 2015]. The cause of these recent declines is a point of contention, in particular, the role of overfishing and declining water quality versus regional-scale processes. There were significant mass-bleaching events in1997/1998 and 2005 and a cold anomaly in the winter of 2010 that together were responsible for considerable mortality [*Lirman et al.*, 2011].

Given the considerable loss of coral in the last 35 years it is relevant to ask if contemporary rates of carbonate production on Caribbean reefs are adequate to maintain the reefal framework and keep up with sea level rise. Over the middle to late Holocene, core records indicate that reefs in the Caribbean maintained vertical accretion rates of 3.6 mm yr^{-1} [*Perry et al.*, 2013]. Making common assumptions about the density (2.9 g cm^{-3}) and porosity (50%), as recommended in *Kinsey* [1985], this accretion translates into a net production rate of ~5 kg $CaCO_3$ m^{-2} yr^{-1}. The present study found that on the FRT, one of the seven transects had a negative annual NCC (Fowey −1.1 kg $CaCO_3$ m^{-2} yr^{-1}) and the other six fell into the low net production range of 0.1–1.0 kg $CaCO_3$ m^{-2} yr^{-1}. Converting these net production rates to vertical accretion rates using the same assumptions used above we obtain 0.07–0.67 mm yr^{-1}. According to the Fifth Intergovernmental Panel on Climate Change Assessment Report sea level is conservatively projected to rise 0.4–1.0 m above the present-day level by the year 2100 [*Church et al.*, 2013]. Obviously, an increase in water depth over the reefs of 0.4–1.0 m is not going to drown any of the reefs in south Florida; however, *Ferrario et al.* [2014] found that water depth at the reefal crest (shallowest point of the reefal profile) was the most important factor determining how much wave energy the reef attenuates (~97%). This means that in coming decades the coastline protection offered by Florida's reefs is going to be degraded as water depth over the reef is increased by 0.4–1.0 m.

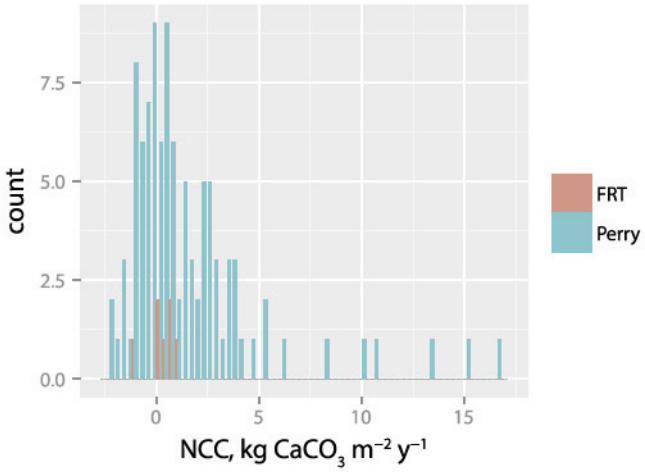

Figure 15. Histogram showing how rates of NCC from the present study for the FRT compare with a study covering the wider Caribbean [*Perry et al.*, 2013].

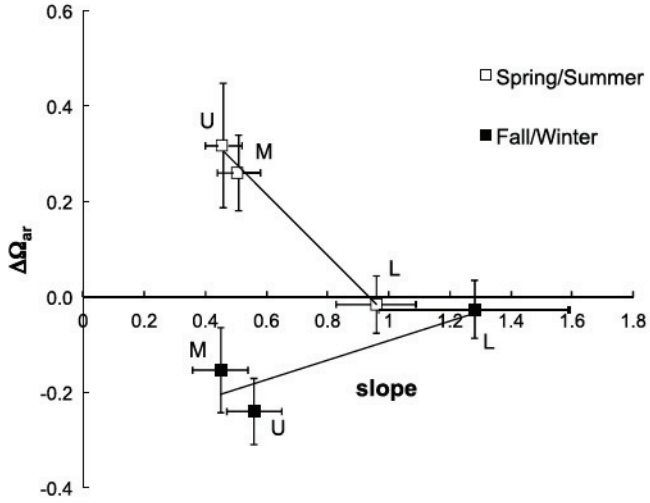

Figure 16. Relationship between the slope of the metabolic vector and the increase (positive feedback) or decline (negative feedback) of Ω_{ar} relative to offshore ocean water. *U*, *M*, and *L* denote upper, middle, and lower Florida Keys. The error bars are ±SEM.

Figure 15 shows how the rates of NCC on the FRT from the present study compare with rates measured across the wider Caribbean in the *Perry et al.* [2013] study. The median from the Perry study was 0.56 kg $CaCO_3$ m^{-2} yr^{-1}, and 50% of the observations fell between −0.41 and +2.43 kg $CaCO_3$ m^{-2} yr^{-1} (based on analysis of the data in the supporting table provided by *Perry et al.* [2013]). In the present study the median for the FRT was 0.47 kg $CaCO_3$ m^{-2} yr^{-1} and 50% of the rates fell between 0.1 and 0.68 kg $CaCO_3$ m^{-2} yr^{-1}. Clearly, the reefs on the FRT are like many other reefs in the Caribbean. They are net depositional but the median rate is just 10% of the historical rate for the region (4.7 kg $CaCO_3$ m^{-2} yr^{-1}) [*Perry et al.*, 2013]. The fact that the northernmost reef was net erosional on an annual basis (−1.1 kg $CaCO_3$ m^{-2} yr^{-1}) and that the next four transects experienced significant seasonal dissolution (Figure 13a) means that these reefs are potentially at risk and should be closely monitored. We note, also, that there was a significant trend for NCC to be higher on the inner (0.57 ± 0.20 kg $CaCO_3$ m^{-2} yr^{-1}) than on the outer reefs (0.16 ± 0.12 kg $CaCO_3$ m^{-2} yr^{-1}). This is consistent with the findings of *Lirman and Fong* [2007] that inshore patch reefs in the Florida Keys have higher coral cover and the corals on them have higher growth rates and lower partial mortality than the offshore reefs. That the inshore patch reefs are in better shape than the offshore reefs suggests that proximity to land and the factors associated with that (nutrient runoff, pollution, and sedimentation) cannot be the first-order cause for the pattern of reefal health that we are observing.

The low rates of net carbonate production on the FRT and the wider Caribbean are to be expected simply due to the roughly 80% decline in coral cover [*Gardner et al.*, 2003]. However, the decline of net calcification relative to historical values may be related to more than coral cover loss. As corals die more and more dead substrate becomes available to colonization by bioeroders, *Eakin* [1996] reported rates of bioerosion as high as −3.65 kg $CaCO_3$ m^{-2} yr^{-1}, following the 1982/1983 mass mortality of corals on Uva Island, Panama, on reefs that were net depositional before the mass mortality event. Other trends may be at work as well. Studies have shown that decreasing pH stimulates the activity of bioeroders [*Enochs et al.*, 2015; *Tribollet et al.*, 2009]. On the Florida Reef Tract, bioerosion is created by echinoderms, euendoliths [*Tribollet and Golubic*, 2011], mollusks [*Lidz and Hallock*, 2000], and encrusting or excavating sponges [*Chiappone et al.*, 2007; *Enochs et al.*, 2015]. Sea grass rhizomes are also known to cause dissolution of carbonate sediments [*Burdige and Zimmerman*, 2002; *Burdige et al.*, 2010]. In the present study we noted that net dissolution was most evident during the fall and winter. We hypothesize that organic matter can build up in winter following the die-off of annual sea grasses (e.g., *Halophila decipiens*) or the leaf-shedding of perennial sea grasses like *Thalassia testudium* [*Zieman et al.*, 1999; *Thayer et al.*, 1982]. The winter standing stock of sea grasses has been estimated as ~15% lower than in summer [*Zieman et al.*, 1999], and the extensive coverage of sea grass beds on the reefal tract could provide a ready supply of decomposing organic detritus [*Thayer et al.*, 1982]. The subsequent oxidation of organic matter can result in pH reductions to ranges of 7.0–7.4 in reefal pore water [*Walter and Burton*, 1990], thereby facilitating the dissolution of calcium carbonate in reefal sediments [*Andersson and Mackenzie*, 2011; *Falter and Sansone*, 2000; *Tribble*, 1993; *Tribble et al.*, 1990]. In the Bahamas Bank, aragonite under saturation was observed at depths as little as 4 cm below the sediment-water interface [*Burdige et al.*, 2010]. As ocean acidification continues, permeable calcium carbonate sediments across the reef may also switch from net precipitating to net dissolving as found by *Cyronak et al.* [2013], thereby affecting net reefal accretion and calcification rates.

Previous work measuring calcification on the Florida Reef Tract has been smaller in spatial and shorter in temporal scales. *Yates and Halley* [2003] deployed a benthic chamber ~10–20 km from our Pennekamp Park transect. Their summer rate of NCC averaged 9.2 ± 8.5 mmol m^{-2} d^{-1} compared to our rate of 13.7 ± 5.5. *Moses et al.* [2009] used benthic habitat maps based on 30 m resolution Landsat 7 Enhanced Thematic Mapper+ imagery to scale up measurements of calcification from habitat-specific measurements made at the 10 m^2 scale to the regional scale (10^3–10^4 km^2 scale) and arrived at a rate of -0.02 mmol m^{-2} d^{-1} for the northern FRT. This compares to our estimate for the upper Florida Keys of -6.8 ± 5.9 mmol m^{-2} d^{-1}. The two estimates agree to within the measurement error.

4.2. Seasonality of Carbonate Chemistry and Relationship to Biological Activity

The seasonality in Ω_{ar} reported in this study was the result of the switch between net photosynthesis during the spring and summer and net respiration during the fall and winter. During the spring and summer the process of calcification partially offsets the increase in Ω_{ar}, and during the fall and winter dissolution partially offsets the decrease in Ω_{ar}. The increase during the spring and summer can be considered a positive feedback that will enhance calcification, and the decrease in Ω_{ar} during the fall and winter can be considered a negative feedback that will depress calcification and increase dissolution. The magnitude of the feedback varied with location in relation to the slope of the TA-DIC metabolic vector (Figure 16). Note that elevation in the spring/summer and the depression in the fall/winter were greatest on the middle and upper Florida Key reefs, where the slopes were very low. While in the lower Keys where the slope was 1.0 to 1.3, there was very little effect on Ω_{ar} and a much weaker seasonality in NCC and no net dissolution during the fall/winter.

The positive biological feedback where DIC drawdown is associated with increased Ω_{ar} has been demonstrated for several coastal environments over diurnal and seasonal time scales [*Suzuki et al.*, 1995; *Semesi et al.*, 2009; *Bates et al.*, 2010] and has been suggested to provide corals with a refuge from ocean acidification [*Kleypas et al.*, 2011; *Manzello et al.*, 2012]. Negative biological feedback resulting when respiration of organic matter causes an increase in DIC has received less mention but may be important in systems that accumulate a lot of organic matter that then breaks down by bacterial action during the fall and winter and depresses Ω_{ar}. During this study, mats of black decaying sea grass were observed on the reefs in the middle and upper Florida Keys during the fall and winter trips. The low NCC:NCP ratios measured in the middle and upper Florida Keys are consistent with the low coral cover now in the 6–8% range [*Vega-Rodriguez et al.*, 2015] and the fact that macroalgae and sea grass beds cover ~56% of the 3141 km^2 of reefal tract [*Lidz et al.*, 2007; *Lirman and Biber*, 2000].

4.3. Relationships Between Net Ecosystem Calcification (NCC), Aragonite Saturation State (Ω_{ar}), and Net Community Production (NCP)

There is great interest in developing a relationship between NCC and Ω_{ar} that will allow predictions to be made of when different reefal systems might be expected to cross a tipping point between net carbonate accretion and net erosion. NCC-Ω_{ar} relationships based on mesocosm experiments containing a carbonate sediment substrate have placed the threshold Ω_{ar} at 1.7 ± 0.3 [*Langdon et al.*, 2000], 2.5 ± 0.4 [*Yates and Halley*, 2006], and 1.46–1.94 [*Andersson et al.*, 2009]. *Leclercq et al.* [2002] found no evidence that the relationship would fall below zero even at $\Omega_{ar} = 0$ in their coral community mesocosm, but interestingly, their sand-only mesocosm had an x intercept of 2.65. Some field studies are reporting threshold Ω_{ar} in the same range as the mesocosm studies, 1.7 ± 0.8 [*Shamberger et al.*, 2011] and 1.2 ± 1.6 [*Shaw et al.*, 2012], but others are reporting significantly higher values, 4.9 [*Ohde and van Woesik*, 1999], 3.4 ± 0.5 [*Silverman et al.*, 2007a], 2.8 ± 1.3 [*Falter et al.*, 2012], 3.2 winter and 3.4 summer [*Albright et al.*, 2013], and 3.6 ± 1.8 (present study). An explanation that remains to be tested is that the differences in the x intercepts are explained by differences in dissolution with the natural systems generally having much higher dissolution than the mesocosms and hence having higher threshold saturation states. In the *Shaw et al.* [2012] study it is interesting to speculate that the rate of dissolution varied seasonally.

There is probably some value in simply averaging all of the threshold values based on field studies and calling that the best guess of the global coral reefal threshold value available today. That value would be 3.0 ± 0.5 (based on the values reported above). However, that begs the question of whether there are real reef-to-reef differences in the threshold that we should know about and understand. Getting to that point

will require understanding why the scatter in the field-based NCC-Ω_{ar} relationships is typically so large and figuring out what can be done to reduce it. The scatter would be reduced if we could improve the precision of the NCC measurements. It could also be reduced by getting a better handle on the environmental factors (light, temperature, nutrients, and food) that covary with Ω_{ar}, which are known to influence the rate of NCC, and hence can confound the interpretation of NCC-Ω_{ar} relationships. An obvious example is light. More studies need to report measurements of light and the relationship between NCC and light. The studies that have included light have found that most of the variability in NCC can be explained by light or NCP (which covaries with light) and very little additional predictive power is gained by including Ω_{ar} [*Falter et al.*, 2012; *Shaw et al.*, 2012; *Albright et al.*, 2013; present study]. This finding does not necessarily mean that Ω_{ar} is not also controlling NCC. It could simply mean that the effect of light or NCP on NCC is masking the effect of Ω_{ar} because the two factors covary. See *Marubini et al.* [2001, Figure 3] for an example of both light and Ω_{ar} simultaneously controlling the rate of NCC of corals. The effect of light on NCC is much stronger than the effect of Ω_{ar}, making it easy to understand how in a field study the effect of light could mask the effect of Ω_{ar}. Increasing the range of Ω_{ar} values would increase the predictive power of NCC-Ω_{ar} relationships because less extrapolation to the threshold will be required. Extrapolation carries the assumption that the relationship remains linear beyond the range constrained by data. This can be achieved by conducting studies over longer periods of time because seasonal variability in Ω_{ar} is generally greater than diel variability. Longer studies are also desirable because few studies have compared the response of NCC to variability in Ω_{ar} on time scales from days to years and shown that the responses are comparable [*Langdon et al.*, 2000, Figure 7].

Another thought on the source of the variability in field-derived NCC-Ω_{ar} relationships is that we are measuring the Ω_{ar} of the bulk water overlying the reef. This may be a good approximation of the Ω_{ar} that the corals and other calcifiers are experiencing, but we know it is not representative of the Ω_{ar} in the environments where dissolution is occurring. In environments where calcification dominates this limitation is less important. However, in environments where the balance between calcification and dissolution is closer to one this limitation may become more extreme and this may be evidenced as a high degree of variability in the relationship between NCC and Ω_{ar} precisely in the region of the relationship that we are most interested. The solution may be not only to continue to relate calcification rates to bulk water Ω_{ar} but also to make efforts in future studies to make measurements of the carbonate chemistry of the interstitial waters and see if that yields a tighter relationship to rates of dissolution. The same studies could also yield relationships between the Ω_{ar} of the overlying bulk water and the profile of Ω_{ar} in the interstitial water.

4.4. Conclusions

The results of this study showed that many of the reefs on the Florida Reef Tract were experiencing significant dissolution during the fall and winter months of 2009 and 2010 and that the northernmost reefs were net erosional on an annual basis during those two years. These results should be cause for alarm. Previous thinking was that reefs would not reach this point until atmospheric pCO_2 reached levels in excess of 500 or even 1000 μatm [*Yates and Halley*, 2006; *Hoegh-Guldberg et al.*, 2007; *Silverman et al.*, 2009; *Andersson et al.*, 2009]. Studies looking at the balance between carbonate production and bioerosion on coral reefs using a census-based approach have also arrived at the conclusion that many reefs in the Caribbean and on the FRT in particular are already net erosional [*Enochs et al.*, 2015; *Perry et al.*, 2013], but this is the first study based on geochemical data that unequivocally provides evidence of widespread carbonate dissolution that appears to be seasonal in nature.

The north-south gradient in dissolution was an interesting feature of this study and should be followed up. Is it a static feature reflecting the fact that the Florida Reef Tract is located at the transition between the tropics and the temperature zone and therefore is located where latitudinal gradients in light, temperature, and Ω_{ar} may exert a strong influence [*Muir et al.*, 2015]? Or does it reflect the influence of human disturbance from the 2.6 million people living in nearby Miami/Dade County? What role is the progressive acidification of the reefal waters playing? It has been well established that the upper Florida Keys are losing corals at a faster rate than the reefs in the middle and lower Florida Keys [*Reich et al.*, 2002]. Lower coral cover means less carbonate production and more, dead substrate available for colonization by bioeroders, a positive feedback that could accelerate the approach to a tipping point in the carbonate balance on coral reefs.

Acknowledgments

This project was funded by National Science Foundation grant OCE 0825578 to Chris Langdon and David Kadko. Additional support to Nancy Muehellhner was provided by a University of Miami Maytag Fellowship and a Marine Technology and Science grant. We thank the captain and crew of the R/V *W. Smith*; Mark Stephens from RSMAS; and Elizabeth Johns, Nelson Melo, Rik Wanninkhof, and Derek Manzello from the Atlantic Oceanographic and Meteorological Laboratory for their assistance with data acquisition. Supporting data for the estimation of water residence time are included in two tables in the supporting information file. A complete set of data files can be found at BCO-DMO (www.bcodmo.org) Project name "Florida Reef Tract NCC and NCP 2009-2010."

References

Albright, R., C. Langdon, and K. R. N. Anthony (2013), Dynamics of seawater carbonate chemistry, production, and calcification of a coral reef flat, Central Great Barrier Reef, *Biogeosci. Discuss.*, *10*(5), 7641–7676, doi:10.5194/bgd-10-7641-2013.

Andersson, A. J., and D. Gledhill (2012), Ocean acidification and coral reefs: Effects on breakdown, dissolution, and net ecosystem calcification, *Annu. Rev. Mar. Sci.*, *5*, 321–348, doi:10.1146/annurev-marine-121211-172241.

Andersson, A. J., and F. T. Mackenzie (2011), Revisiting four scientific debates in ocean acidification research, *Biogeosciences*, *9*(3), 893–905, doi:10.5194/bg-9-893-2012.

Andersson, A. J., N. Bates, and F. Mackenzie (2007), Dissolution of carbonate sediments under rising pCO_2 and ocean acidification: Observations from Devil's Hole, Bermuda, *Aquat. Geochem.*, *13*, 237–264, doi:10.1007/s10498-007-9018-8.

Andersson, A. J., I. B. Kuffner, F. T. Mackenzie, P. L. Jokiel, K. S. Rogers, and A. Tan (2009), Net loss of $CaCO_3$ from a subtropical calcifying community due to seawater acidification: Mesocosm-scale experimental evidence, *Biogeosci. Discuss.*, *6*, 1811–1823, doi:10.5194/bg-6-1811-2009.

Atkinson, M. J., and P. Cuet (2008), Possible effects of ocean acidification on coral reef biogeochemistry, *Mar. Ecol. Prog. Ser.*, *373*, 249–256, doi:10.3354/meps07867.

Barnes, D. J., and M. J. Devereux (1984), Productivity and calcification on a coral reef: A survey using pH and oxygen electrode techniques, *J. Exp. Mar. Biol. Ecol.*, *79*, 213–231, doi:10.1016/0022-0981(84)90196-5.

Bates, N. R., A. Amati, and A. J. Andersson (2010), Feedbacks and responses of coral calcification on the Bermuda reef system to seasonal changes in biological processes and ocean acidification, *Biogeosciences*, *7*, 2509–2530, doi:10.5194/bg-7-2509-2010.

Bates, N. R., M. Best, K. Neely, R. Garley, A. G. Dickson, and R. J. Johnson (2012), Detecting anthropogenic carbon dioxide uptake and ocean acidification in the North Atlantic Ocean, *Biogeosciences*, *9*, 2509–2522.

Brewer, P. G., and J. C. Goldman (1976), Alkalinity changes generated by phytoplankton growth, *Limnol. Oceanogr.*, *21*, 108–117, doi:10.4319/lo.1976.21.1.0108.

Burdige, D. J., and R. C. Zimmerman (2002), Impact of sea grass density on carbonate dissolution in Bahamian sediments, *Limnol. Oceanogr.*, *47*, 1751–1763, doi:10.4319/lo.2002.47.6.1751.

Burdige, D. J., X. Hun, and R. C. Zimmerman (2010), The widespread occurrence of coupled carbonate dissolution/reprecipitation in surface sediments on the Bahamas Bank, *Am. J. Sci.*, *310*, 492–521, doi:10.2475/06.2010.03.

Burman, S. G., R. B. Aronson, and R. van Woesik (2012), Biotic homogenization of coral assemblages along the Florida Reef Tract, *Mar. Ecol. Prog. Ser.*, *467*, 89–96, doi:10.3354/meps09950.

Cai, W.-J., X. Hu, W.-J. Huang, L.-Q. Jiang, Y. Wang, T.-H. Peng, and X. Zhang (2010), Alkalinity distribution in the western North Atlantic Ocean margins, *J. Geophys. Res.*, *115*, C08014, doi:10.1029/2009JC005482.

Chan, N. C. S., and S. R. Connolly (2013), Sensitivity of coral calcification to ocean acidification: A meta-analysis, *Global Change Biol.*, *19*, 282–290, doi:10.1111/gcb.12011.

Chiappone, M., L. M. Rutten, S. L. Miller, and D. W. Swanson (2007), Large-scale distributional patterns of the encrusting and excavating sponge *Cliona delitrix* Pang on Florida Keys coral substrates, in *Proc 7th Int Sponge Symp. on Porifera Research: Biodiversity, Innovation and Sustainability*, *Sér. Livros*, vol. 2, edited by M. R. Custodio et al., pp. 255–263, Museu Nacional, Rio de Janeiro, Braz., doi:10.1111/j.1439-0485.2010.00416.x.

Church, J. A., et al. (2013), Sea level change, in *Climate Change 2013: The Physical Science Basis Contribution of Working Group I to the Fifth Assessment Report of the Intergovernmental Panel on Climate Change*. edited by T. F. Stocker et al., chap. 13, pp. 1137–1216, Cambridge Univ. Press, Cambridge, U. K., doi:10.1126/science.342.6165.1445-a.

Cubit, J. D., H. A. Lessios, and D. R. Robertson (1984), Spread of *Diadema* mass mortality through the Caribbean, *Science*, *226*, 335–337, doi:10.1126/science.226.4672.335.

Cyronak, T., I. R. Santos, and B. D. Eyre (2013), Permeable coral reef sediment dissolution driven by elevated pCO_2 and pore water advection, *Geophys. Res. Lett.*, *40*(18), 4876–4881.

Dickson, A. G. (1990), Standard potential of the reaction: $AgCl(s) + OH_2(g) = Ag(s) + HCl(aq)$, and the standard acidity constant of the ion HSO_4 in synthetic seawater from 273.15 to 318.15 K, *J. Chem. Thermodyn.*, *22*, 113–127, doi:10.1016/0021-9614(90)90074-z.

Dickson, A. G., and F. J. Millero (1987), A comparison of the equilibrium constants for the dissociation of carbonic acid in seawater media, *Deep Sea Res., Part I*, *34*, 1733–1743, doi:10.1016/0198-0149(87)90021-5.

Dickson, A. G., J. D. Afghan, and G. C. Anderson (2003), Reference materials for oceanic CO_2 analysis: A method for the certification of total alkalinity, *Mar. Chem.*, *80*(2-3), 185–197, doi:10.1016/s0304-4203(02)00133-0.

Dickson, A. G., C. L. Sabine, and J. R. Christian (2007), *Guide to Best Practices for Ocean CO_2 Measurements*, *PICES Spec. Publ.*, vol. 3, 176 pp., North Pacific Marine Science Organization, Sidney, B. C., doi:10.2172/885672.

Eakin, C. M. (1996), Where have all the carbonates gone? A model comparison of calcium carbonate budgets before and after the 1982–1983 El Niño at Uva Island in the eastern Pacific, *Coral Reefs*, *15*, 109–119, doi:10.1007/bf01771900.

Enochs, I. C., D. P. Manzello, R. D. Carlton, D. M. Graham, R. Ruzicka, and M. A. Colella (2015), Ocean acidification enhances the bioerosion of a common coral reef sponge: Implications for the persistence of the Florida Reef Tract, *Bull. Mar. Sci.*, *91*(2), 271–290, doi:10.5343/bms.2014.1045.

Falter, J. L., and F. J. Sansone (2000), Shallow pore water sampling in reef sediments, *Coral Reefs*, *19*(1), 93–97, doi:10.1007/s003380050233.

Falter, J. L., R. J. Lowe, M. J. Atkinson, and P. Cuet (2012), Seasonal coupling and de-coupling of net calcification rates from coral reef metabolism and carbonate chemistry at Ningaloo Reef, Western Australia, *J. Geophys. Res.*, *117*, C05003, doi:10.1029/2011JC007268.

Ferrario, F., M. W. Beck, C. D. Storlazzi, F. Micheli, C. C. Shepard, and L. Airoldi (2014), The effectiveness of coral reefs for coastal hazard risk reduction and adaptation, *Nat. Commun.*, *5*, doi:10.1038/ncomms4794.

Gardner, T. A., I. M. Cote, J. A. Gill, A. Grant, and A. R. Watkinson (2003), Long-term region-wide declines in Caribbean corals, *Science*, *301*(5635), 958–960, doi:10.1126/science.1086050.

Gladfelter, W. B. (1982), White-band disease in *Acropora palmata*: Implications for the structure and growth of shallow reefs, *Bull. Mar. Sci.*, *32*(2), 639–643, doi:10.1007/s00338-007-0278-y.

Ho, D. T., C. S. Law, M. J. Smith, P. Schlosser, M. Harvey, and P. Hill (2006), Measurement of air-sea gas exchange at high wind speeds in the Southern Ocean: Implications for global parameterizations, *Geophys. Res. Lett.*, *33*, L20604, doi:10.1029/2006GL028295.

Hoegh-Guldberg, O., et al. (2007), Coral reefs under rapid climate change and ocean acidification, *Science*, *318*, 1737–1742.

Kadko, D., and D. Olson (1996), Be-7 as a tracer of surface water seduction and mixed layer history, *Deep Sea Res.*, *43*, 89–116, doi:10.1016/0967-0637(96)00011-8.

Kawahata, H., A. Suzuki, and K. Goto (1997), Coral reef ecosystems as a source of atmospheric CO_2: Evidence from pCO_2 measurements of surface waters, *Coral Reefs*, *16*, 261–266, doi:10.1007/s003380050082.

Kinsey, D. D. (1985), Metabolism, calcification and carbon production. I. System level studies, in *Proceedings of the 5th International Coral Reef Congress*, vol. 4, pp. 503–542, ISRS, Tahiti.

Kinsey, D. W. (1978), Productivity and calcification estimates using slack-water periods and field enclosures, in *Coral Reefs: Research Methods, Monogr. Oceanogr. Methods*, vol. 5, pp. 439–468, UNESCO, Paris.

Kleypas, J. A., K. R. N. Anthony, and J.-P. Gattuso (2011), Coral reefs modify their seawater carbon chemistry—Case study from a barrier reef (Moorea, French Polynesia), *Global Change Biol., 17*(12), 3667–3678, doi:10.1111/j.1365-2486.2011.02530.x.

Koch, M., G. Bowes, C. Ross, and X.-H. Zhang (2012), Climate change and ocean acidification effects on seagrasses and marine macroalgae, *Global Change Biol., 19*, 103–132, doi:10.1111/j.1365-2486.2012.02791.x.

Langdon, C., T. Takahashi, C. Sweeney, D. Chipman, J. Goddard, F. Marubini, H. Aceves, H. Barnett, and M. J. Atkinson (2000), Effect of calcium carbonate saturation state on the calcification rate of an experimental coral reef, *Global Biogeochem. Cycles, 14*, 639–654, doi:10.1029/1999GB001195.

Leclercq, N., J.-P. Gattuso, and J. Jaubert (2002), Primary production, respiration, and calcification of a coral reef mesocosm under increased CO_2 partial pressure, *Limnol. Oceanogr., 47*, 558–564, doi:10.4319/lo.2002.47.2.0558.

Lee, T. N., and E. Williams (1999), Mean distribution and seasonal variability of coastal currents and temperature in the Florida Keys with implications for larval recruitment, *Bull. Mar. Sci., 64*, 35–56, doi:10.1007/s00227-008-1082-0.

Lee, T. N., E. Williams, E. Johns, D. Wilson, and N. P. Smith (2002), Transport processes linking south Florida coastal ecosystems, in *The Everglades, Florida Bay and Coral Reefs of the Florida Keys*, edited by J. W. Porter and K. G. Porter, pp. 309–340, CRC Press, Boca Raton, Fla., doi:10.1201/9781420039412-15.

Leichter, J. J., H. L. Stewart, and S. L. Miller (2003), Episodic nutrient transport to Florida coral reefs, *Limnol. Oceanogr., 48*(4), 1394–1407.

Lewis, E., and D. Wallace (1998), *Program Developed for CO_2 System Calculations*, U.S. Department of Energy, Oak Ridge National Laboratory Environmental Sciences Division, Oak Ridge Tenn., doi:10.3334/cdiac/otg.co2sys_dos_cdiac105.

Lidz, B. H., and P. Hallock (2000), Sedimentary petrology of a declining reef ecosystem, Florida Reef Tract (USA), *J. Coastal Res., 16*, 675–697. [Available at http://www.jstor.org/stable/4300079.]

Lidz, B., C. D. Reich, and E. A. Shinn (2007), Systematic mapping of bedrock and habitats along the Florida Reef Tract: central Key Largo to Halfmoon Shoal (Gulf of Mexico), *U.S. Geol. Surv. Prof. Pap., 1751*. [Available at http://pubs.usgs.gov/pp/2007/1751.]

Lirman, D., and P. Biber (2000), Seasonal dynamics of macroalgal communities of the northern Florida Reef Tract, *Bot. Mar., 43*(4), 305–314, doi:10.1515/bot.2000.033.

Lirman, D., and P. Fong (2007), Is proximity to land-based sources of coral stressors an appropriate measure of risk to coral reefs? An example from the Florida Reef Tract, *Mar. Pollut. Bull., 54*(6), 779–791, doi:10.1016/j.marpolbul.2006.12.014.

Lirman, D., et al. (2011), Severe 2010 cold-water event caused unprecedented mortality to corals of the Florida Reef Tract and reversed previous survivorship patterns, *PLoS One, 6*(8), e23047, doi:10.1371/journal.pone.0023047.

Manzello, D. P., J. A. Kleypas, D. A. Budd, C. M. Eakin, P. W. Glynn, and C. Langdon (2008), Poorly cemented coral reefs of the eastern tropical Pacific: Possible insights into reef development in a high-CO_2 world, *Proc. Natl. Acad. Sci. U.S.A., 105*, 10,450–10,455, doi:10.1073/pnas.0712167105.

Manzello, D. P., I. C. Enochs, N. Melo, D. K. Gledhill, and E. M. Johns (2012), Ocean acidification refugia of the Florida Reef Tract, *PLoS One, 7*(7), e41715, doi:10.1371/journal.pone.0041715.

Marubini, F., H. Barnett, C. Langdon, and M. J. Atkinson (2001), Dependence of calcification on light and carbonate ion concentration for the hermatypic coral *Porites compressa*, *Mar. Ecol. Prog. Ser., 220*, 153–162, doi:10.3354/meps220153.

Mehrbach, C., C. H. Culberson, J. E. Hawley, and R. M. Pytkowicz (1973), Measurement of the apparent dissociation constants of carbonic acid in seawater at atmospheric pressure, *Limnol. Oceanogr., 18*, 897–907, doi:10.4319/lo.1973.18.6.0897.

Moses, C. S., S. Andrefouet, C. J. Kranenburg, and F. E. Muller-Karger (2009), Regional estimates of reef carbonate dynamics and productivity using Landsat 7 ETM+, and potential impacts from ocean acidification, *Mar. Ecol. Prog. Ser., 380*, 103–115, doi:10.3354/meps07920.

Muir, P. R., C. C. Wallace, T. Done, and J. D. Aguirre (2015), Limited scope for latitudinal extension of reef corals, *Science, 348*(6239), 1135–1138, doi:10.1126/science.1259911.

Ohde, S., and R. van Woesik (1999), Carbon dioxide flux and metabolic processes of a coral reef, Okinawa, *Bull. Mar. Sci., 65*, 559–576.

Perry, C. T., G. N. Murphy, P. S. Kench, S. G. Smithers, E. N. Edinger, R. S. Steneck, and P. J. Mumby (2013), Caribbean-wide decline in carbonate production threatens coral reef growth, *Nat. Commun., 4*, 1402, doi:10.1038/ncomms2409.

Reich, C. D., E. A. Shinn, T. D. Hickey, and A. B. Tihansky (2002), Tidal and meteorological influences on shallow marine groundwater flow in the Upper Florida Keys, in *The Everglades, Florida Bay and Coral Reefs of the Florida Keys*, edited by J. W. Porter and K. G. Porter, pp. 749–770, CRC Press, Boca Raton, Fla., doi:10.1201/9781420039412-30.

Sabine, C. L., et al. (2004), The oceanic sink for anthropogenic CO_2, *Science, 305*, 367–371, doi:10.1126/science.1097403.

Semesi, I. S., S. Beer, and M. Björk (2009), Seagrass photosynthesis controls rates of calcification and photosynthesis of calcareous macroalgae in a tropical seagrass meadow, *Mar. Ecol. Prog. Ser., 382*, 41–47, doi:10.3354/meps07973.

Shamberger, K. E. F., R. A. Feely, C. L. Sabine, M. J. Atkinson, E. H. DeCarlo, F. T. Mackenzie, P. S. Drupp, and D. A. Butterfield (2011), Calcification and organic production on a Hawaiian coral reef, *Mar. Chem., 127*, 64–75, doi:10.1016/j.marchem.2011.08.003.

Shaw, E. C., B. I. McNeil, and B. Tilbrook (2012), Impacts of ocean acidification in naturally variable coral reef flat ecosystems, *J. Geophys. Res., 117*, C03038, doi:10.1016/j.marchem.2011.08.003.

Silverman, J., B. Lazar, and J. Erez (2007a), Effect of aragonite saturation, temperature, and nutrients on the community calcification rate of a coral reef, *J. Geophys. Res., 112*, C05004, doi:10.1029/2006JC003770.

Silverman, J., B. Lazar, and J. Erez (2007b), Community metabolism of a coral reef exposed to naturally varying dissolved inorganic nutrient loads, *Biogeochemistry, 84*, 67–82, doi:10.1007/s10533-007-9075-5.

Silverman, J., B. Lazar, L. Cao, K. Caldiera, and J. Erez (2009), Coral reefs may start dissolving when atmospheric CO_2 doubles, *Geophys. Res. Lett., 36*, L05606, doi:10.1029/2008GL036282.

Silverman, J., D. I. Kline, L. Johnson, T. Rivlin, K. Schneider, J. Erez, B. Lazar, and K. Caldeira (2012), Carbon turnover rates in the One Tree Island reef: A 40-year perspective, *J. Geophys. Res., 117*, G03023, doi:10.1029/2012JG001974.

Smith, S. V., and G. S. Key (1975), Carbon dioxide and metabolism in marine environments, *Limnol. Oceanogr., 20*, 493–495, doi:10.4319/lo.1975.20.3.0493.

Smith, S. V., and M. J. Atkinson (1983), Mass balance of carbon and phosphorus in Shark Bay, Western Australia, *Limnol. Oceanogr., 28*, 625–639.

Soto, I. M., F. E. Muller-Karger, P. Hallock, and C. Hu (2011), Sea surface temperature variability in the Florida Keys and its relationship to coral cover, *J. Mar. Biol.*, doi:10.1155/2011/981723.

Suzuki, A., T. Nakamori, and H. Kayanne (1995), The mechanism of production enhancement in coral reef carbonate systems: Model and empirical results, *Sediment. Geol., 99*, 259–280, doi:10.1016/0037-0738(95)00048-d.

Suzuki, A., T. Nakamori, and H. Kayanne (2003), Carbon budget of coral reef systems: An overview of observations in fringing reefs, barrier reefs and atolls in the Indo-Pacific regions, *Tellus, Ser. B, 55*, 428–444, doi:10.1034/j.1600-0889.2003.01442.x.

Szmant, A. M., and A. Forrester (1996), Water column and sediment nitrogen and phosphorus distribution patterns in the Florida Keys, USA, *Coral Reefs*, *15*(1), 21–41, doi:10.1007/bf01626075.

Taylor, C. B., and H. B. Stewart (1959), Summer upwelling along the east coast of Florida, *J. Geophys. Res.*, *64*(1), 33–40, doi:10.1029/JZ064i001p00033.

Thayer, G. W., D. W. Engel, and K. A. Bjorndal (1982), Evidence for short-circuiting of the detritus cycle of seagrass beds by the green turtle, *Chelonia mydas*, *J. Exp. Mar. Biol. Ecol.*, *62*, 173–183, doi:10.1016/0022-0981(82)90090-9.

Tribble, G. W. (1993), Organic matter oxidation and aragonite diagenesis in a coral reef, *J. Sediment. Res.*, *63*, 523–527, doi:10.1306/d4267b45-2b26-11d7-8648000102c1865d.

Tribble, G. W., F. J. Sansone, and S. V. Smith (1990), Stoichiometric modeling of carbon diagenesis within a coral reef framework, *Geochm. Cosmochim. Acta*, *54*, 2439–2449, doi:10.1016/0016-7037(90)90231-9.

Tribollet, A., and S. Golubic (2011), Reef bioerosion: Agents and processes, in *Coral Reefs: An Ecosystem in Transition*, edited by Z. Dubinsky and N. Stambler, pp. 435–449, Springer, Dordrecht, Netherlands, doi:10.1007/978-94-007-0114-4_25.

Tribollet, A., C. Godinot, M. Atkinson, and C. Langdon (2009), Effects of elevated pCO_2 on dissolution of coral carbonates by microbial euendoliths, *Global Biogeochem. Cycles*, GB3008, *23*, doi:10.1029/2008GB003286.

Vega-Rodriguez, M., et al. (2015), Influence of water-temperature variability on stony coral diversity in Florida Keys patch reefs, *Mar. Ecol. Prog. Ser.*, *528*, 173–186, doi:10.3354/meps11268.

Venti, A., D. Kadko, A. J. Andersson, C. Langdon, and N. R. Bates (2012), A multi tracer model approach to estimate reef water residence times, *Limnol. Oceanogr. Methods*, *10*, 1078–1005, doi:10.4319/lom.2012.10.1078.

Walter, L. M., and E. A. Burton (1990), Dissolution of recent platform carbonate sediments in marine pore fluids, *Am. J. Sci.*, *290*, 601–643, doi:10.2475/ajs.290.6.601.

Watanabe, A., H. Kayanne, H. Hata, S. Kudo, K. Nozaki, K. Kato, A. Negishi, Y. Ikeda, and H. Yamano (2006), Analysis of the seawater CO_2 system in the barrier reef-lagoon system of Palau using total alkalinity-dissolved inorganic carbon diagrams, *Limnol. Oceanogr.*, *51*, 1614–1628, doi:10.4319/lo.2006.51.4.1614.

Yates, K. K., and R. B. Halley (2003), Measuring coral reef community metabolism using new benthic chamber technology, *Coral Reefs*, *22*, 247–255, doi:10.1007/s00338-003-0314-5.

Yates, K. K., and R. B. Halley (2006), CO_3^{2-}, concentration and pCO_2 thresholds for calcification and dissolution on the Molokai reef flat, Hawaii, *Biogeosciences*, *3*(3), 357–369, doi:10.1016/j.marchem.2006.12.008.

Zieman, J. C., J. W. Fourqurean, and T. A. Frankovich (1999), Seagrass die-off in Florida Bay: Long-term trends in abundance and growth of turtle grass, *Thalassia testudinum*, *Estuaries*, *22*, 460–470, doi:10.2307/1353211.